

# Continuous-time state-space methods for $\delta^{18}\text{O}$ and $\delta^{13}\text{C}$

Mikkel Bennedsen<sup>(a)</sup>, Eric Hillebrand<sup>(a\*)</sup>, Siem Jan Koopman<sup>(b)</sup>, Kathrine Larsen<sup>(a)</sup>

Authors in alphabetical order

<sup>(a)</sup>Department of Economics and Business Economics, Aarhus University, Denmark.

<sup>(a\*)</sup>Corresponding author: ehillebrand@econ.au.dk

<sup>(c)</sup>Department of Econometrics, Vrije Universiteit Amsterdam, The Netherlands

April 9, 2024

## Abstract

Time series analysis of  $\delta^{18}\text{O}$  and  $\delta^{13}\text{C}$  measurements from benthic foraminifera for purposes of paleoclimatology is challenging. The time series reach back tens of millions of years, they are relatively sparse in the early record and relatively dense in the later, the time stamps of the observations are not evenly spaced, and there are instances of multiple different observations at the same time stamp. The time series appear non-stationary over most of the historical record with clearly visible temporary trends of varying directions. In this paper, we propose a continuous-time state-space framework to analyze the time series. State space models are uniquely suited for this purpose, since they can accommodate all the challenging features mentioned above. We specify univariate models and joint bivariate models for the two time series of  $\delta^{18}\text{O}$  and  $\delta^{13}\text{C}$ . The models are estimated using maximum likelihood by way of the Kalman filter recursions. The suite of models we consider has an interpretation as an application of the Butterworth filter. We propose model specifications that take the origin of the data from different studies into account and that allow for a partition of the total period into sub-periods reflecting different climate states. The models can be used, for example, to impute evenly time-stamped values by way of Kalman filtering. They can also be used, in future work, to analyze the relation to proxies for CO<sub>2</sub> concentrations.

## 1 Introduction

Measurements of the deviation in the ratio of the oxygen isotopes  $^{18}\text{O}$  and  $^{16}\text{O}$  in ocean sediment cores containing fossil benthic foraminifera allow for obtaining a time series record covering the Cenozoic, i.e., the last 66 million years (Westerhold et al., 2020; Zachos et al., 2001). Since the ratio of the isotopes depends on prevailing temperatures and the amount of water locked in ice sheets at the time of formation of the shell, these measurements can serve as a proxy for global temperatures. Similarly, deviations in the ratio of the carbon isotopes  $^{13}\text{C}$  and  $^{12}\text{C}$  are used as a proxy for the abundance of vegetation.

In this paper, we propose a class of state space models for the time series of  $\delta^{18}\text{O}$  and  $\delta^{13}\text{C}$ . This class of models addresses the central challenges that the time series pose: non-stationarity with trends in changing directions, irregular spacing of the time stamps of the observations, multiple observations at certain time stamps, different studies of origin of the data, different climate states covered by the data, and covariation in the two series, so that one can inform the estimation of a model for the other. The models are specified and estimated by maximum

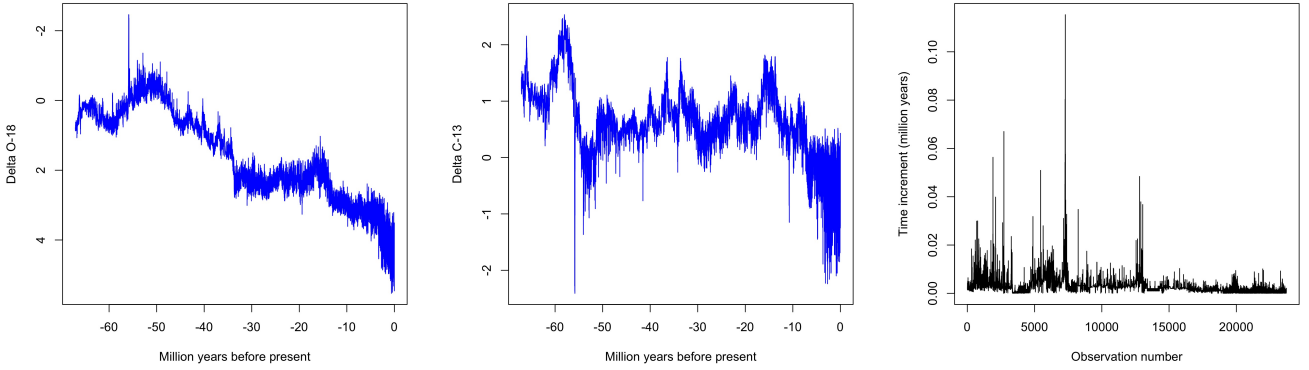


Figure 1: Left panel:  $\delta^{18}\text{O}$  data, middle panel:  $\delta^{13}\text{C}$  data, right panel: Time series of differences in the time stamp. Note that the  $y$ -axis for  $\delta^{18}\text{O}$  is reversed, following common practice.

likelihood in the time domain, and they have a direct interpretation as Butterworth filters in the frequency domain (Gómez, 2001; Harvey and Trimbur, 2003). Their theory is well developed, see, for example, Harvey (1989) and Durbin and Koopman (2012) for textbook treatments, and they can be estimated in relatively short time on laptop computers.

The data set employed in this paper is provided in the study by Westerhold et al. (2020), where  $\delta^{18}\text{O}$  and  $\delta^{13}\text{C}$  measurements from 34 different studies are collated and harmonized in a single data file. This file contains 24321 time-stamped lines. The time stamps range from 67.10113 million years ago (MYA) to 0.000564 MYA. In this paper, we ignore uncertainty in the time stamps. We order the observations such that the series start at -67.10113 million years and end at -0.000564 million years. Of the 24321 time stamps, 23722 are unique, meaning that there are 599 time stamps with more than one observation on either or both of the series.

We use the correlation-corrected observations (column L “benthic d18O VPDB Corr” and column K “benthic d13C VPDB Corr”) from the data file, for which there are four time stamps for which neither  $\delta^{18}\text{O}$  nor  $\delta^{13}\text{C}$  are available (unique observation numbers 19043, 19054, 19057, 21089; data file observation numbers 2823, 4895, 4898, 4909). The maximum number of observations at any time stamp is four, often, but not always, originating from different studies.

Figure 1 shows the time series of  $\delta^{18}\text{O}$  (left panel) and  $\delta^{13}\text{C}$  (middle panel). The right panel shows the time series of differences in the time stamps of the observations in million years. The smallest difference that occurs is a single year (unique obs. no. 22130, data file obs. no. 1778), the biggest is 115366 years (unique obs. no. 7287, data file obs. no. 16932). The plot in the right panel of Figure 1 shows that the data set is denser in the later part of the record and sparser in the earlier, as to be expected.

We show that a data set as complex as this can be analyzed by means of state space methods tailored to the continuous-time nature of the time stamps. Specifically, we employ so-called unobserved component models, and we specify the time series under study as consisting of a latent component we aim to estimate plus measurement noise (Harvey and Koopman, 2000, 2009). Multiple alternative measurements can occur. The Kalman filtering and smoothing recursions allow for the extraction of this unobserved component.

We consider several alternative models that differ in the integration order of the unobserved component. In the simplest case, the random-walk-plus-noise model, the unobserved component is a random walk, that is, integrated of order one. This stochastic trend is a flexible structure that can accommodate the changing trend directions in the series and, at the same time, allow for specifying a non-stationary time series model. With increasing orders of integration of the latent component, the degree of smoothing of the extracted component increases. We describe the relation of the integration orders to orders of a Butterworth filter applied in the frequency

domain, and we show the gain functions implied by the maximum likelihood estimation of our time-domain models (Gómez, 1999, 2001; Harvey and Trimbur, 2003).

The separate specification of measurement and transition equations in a state space model, with their own respective error processes, allows for reflecting the different sources of the data (34 different studies, or, alternatively, 23 different benthic foraminifera species), by way of specifying different measurement equation variances. The variances of the random variables that drive the transition equation are differentiated according to the six different climate states identified in Westerhold et al. (2020). We consider bivariate models for  $\delta^{18}\text{O}$  and  $\delta^{13}\text{C}$  jointly, such that we can exploit their covariation to inform the estimation of our models.

The rest of the paper is organized as follows: In Section 2, we apply random-walk-plus-noise models to the data set, both without and with differentiating variances. We consider univariate and bivariate specifications. In Section 3, we describe the relation of unobserved component models with the Butterworth filter. In Section 4, we explore higher integration orders of the unobserved component, which correspond to higher orders of Butterworth filters. Section 6 concludes.

## 2 Random walk plus noise models

We propose the class of unobserved component models for  $\delta^{18}\text{O}$  and  $\delta^{13}\text{C}$ , since these models can accommodate non-stationarity, unevenly spaced observations, missing data, and multiple observations for the same object of interest. Unobserved component models can be written in univariate form as

$$y_t = \mu_t + \psi_t,$$

where  $\mu_t$  is the “unobserved component” of interest that is observed with a random error  $\psi_t$ . The time index  $t$  is an element of an ordered set that can be evenly or unevenly spaced. We can think of  $\mu_t$  as the “signal” and  $\psi_t$  as the “noise”.

The simplest specification in this class that we are going to consider for the two time series studied here is the random walk plus noise model

$$\begin{aligned} y_t &= \mu_t + \varepsilon_t, & \varepsilon_t &\stackrel{i.i.d.}{\sim} \text{N}(0, \sigma_\varepsilon^2), \\ \mu_{t+\Delta t} &= \mu_t + \eta_t, & \eta_t &\stackrel{i.i.d.}{\sim} \text{N}(0, \sigma_\eta^2 \Delta t), \end{aligned} \quad (1)$$

$t = \sum_{s < t} \Delta s$ . In this case  $\psi_t = \varepsilon_t$  is simply an identically and independently distributed normal random variable. The “signal”  $\mu_t$  is a random walk and thus non-stationary. The time increment  $\Delta t$  is varying with time. As an example, the first three and the last three observations in the  $\delta^{18}\text{O}$  and  $\delta^{13}\text{C}$  series are shown in Table 1, where the time increments are reported in the third column. The variance of a random walk and its continuous-time counterpart Brownian motion scales with time (e.g. Karatzas and Shreve, 1991, p. 47). The variance of an increment of Brownian motion  $\sigma B_t$  is given by

$$\mathbb{E}[\sigma(B_t - B_s)]^2 = \sigma^2(t - s), \quad 0 \leq s < t,$$

and this motivates our definition of the variance of  $\eta_t$ . Loosely speaking, the random variable  $\eta_t$  captures the variation occurring in the process  $\mu_t$  in the time interval  $[t, t + \Delta t]$ , and so if  $\mu_t$  is to model a random walk, its variance on this increment must be  $\sigma_\eta^2 \Delta t$ .

Model (1) can be estimated by maximum likelihood derived from the distribution assumptions. The evaluation of the likelihood is a byproduct of the Kalman filter recursions, see Durbin and Koopman (2012), in particular Ch. 7, for a textbook treatment. The first equation in model (1) constitutes a measurement equation and the second a transition equation of a state space model. The state variable  $\mu_t$  is unobserved and inferred from observations  $y_t$ . The parameters to be estimated by maximum likelihood are  $\sigma_\varepsilon^2$  and  $\sigma_\eta^2$ . Estimates of the unobserved state  $\mu_t$  can be

Table 1: First three and last three observations of the  $\delta^{18}\text{O}$  and  $\delta^{13}\text{C}$  time series with time stamps and time increments. The data are from the accompanying data file of Westerhold et al. (2020), file name `aba6853_tables_s8_s34.xlsx`, tab “Table S33”, column L “benthic d18O VPDB Corr” and column K “benthic d13C VPDB Corr”. The data are sorted according to the time stamp in column D “age\_tuned”.

Obs	Obs (data file)	time (MYA)	$\Delta t$	$\delta^{18}\text{O}$	$\delta^{13}\text{C}$
1	24321	67.101133	NA	0.800	1.376
2	24320	67.098975	0.002158	0.800	1.343
3	24319	67.096818	0.002157	0.800	1.320
$\vdots$		$\vdots$	$\vdots$	$\vdots$	$\vdots$
23720	3	0.003099	0.001032	3.56	-0.07
23721	2	0.002689	0.000410	3.57	0.43
23722	1	0.000564	0.002125	3.52	-0.80

Table 2: Maximum likelihood parameter estimates for model (1). Standard errors in parentheses. BIC: Bayes information criterion.

	$\delta^{18}\text{O}$	$\delta^{13}\text{C}$
$\hat{\sigma}_\eta^2$	1.8364 (0.0480)	1.2135 (0.0403)
$\hat{\sigma}_\varepsilon^2$	0.0205 (0.0002)	0.0340 (0.0004)
log-likelihood	7218.57	2992.10
BIC	-14416.99	-5964.05

obtained in predicted form ( $\mathbb{E}[\mu_{t+\Delta t}|\{y_s, s \leq t\}]$ ), filtered form ( $\mathbb{E}[\mu_{t+\Delta t}|\{y_s, s \leq t+\Delta t\}]$ ), and smoothed form ( $\mathbb{E}[\mu_{t+\Delta t}|\{y_s, s \leq \sum \Delta t\}]$ ) from the Kalman filtering and smoothing recursions.

We implement the model with diffuse initialization for the non-stationary state process  $\mu_t$  in the KFAS package in R (Helske, 2017, 2019) and in OxMetrics/SsfPack (Doornik, 2021).

Figure 2 shows the data for  $\delta^{18}\text{O}$  and  $\delta^{13}\text{C}$  together with the smoothed values of  $\mu_t$  from the Kalman smoothing recursions in the top row. The bottom row shows the standardized prediction residuals from the maximum likelihood estimation (Durbin and Koopman, 2012, p. 38, eq. (2.65)). Clearly, these are not i.i.d. with constant variance, and while the standard errors obtained in the estimation give some sense of the dispersion of the parameter estimate, they cannot be interpreted in the sense of a central limit theorem. With this caveat, the maximum likelihood estimates of model (1) are reported in Table 2. The Bayes information criterion is a measure of the fit that penalizes for the number of parameters. This becomes important when we increase the complexity of the model in the following.

## 2.1 Differentiating measurement equation variances according to studies and species

The data set prepared in Westerhold et al. (2020) originates from 34 different sources, according to the data file (column “benthic Source” in tab “Table S33” of the file `aba6853_tables_s8_s34.xlsx`). It seems plausible that the measurement error variance is at least in part dependent on the source the data was taken from. This dependence is implemented in model (1) by modifying the measurement equation to

$$y_{i,t} = \mu_t + \varepsilon_{i,t}, \quad \varepsilon_{i,t} \stackrel{i.i.d.}{\sim} \mathbf{N}(0, \sigma_{\varepsilon,i}^2), \quad i = 1, \dots, 34, \quad (2)$$

where  $i$  indicates the study of origin of a given data point. This generalization of the measurement equation extends the parameter vector to be estimated by maximum likelihood to 35 coordinates (the 34  $\sigma_{\varepsilon,i}^2$  plus  $\sigma_\eta^2$ ).

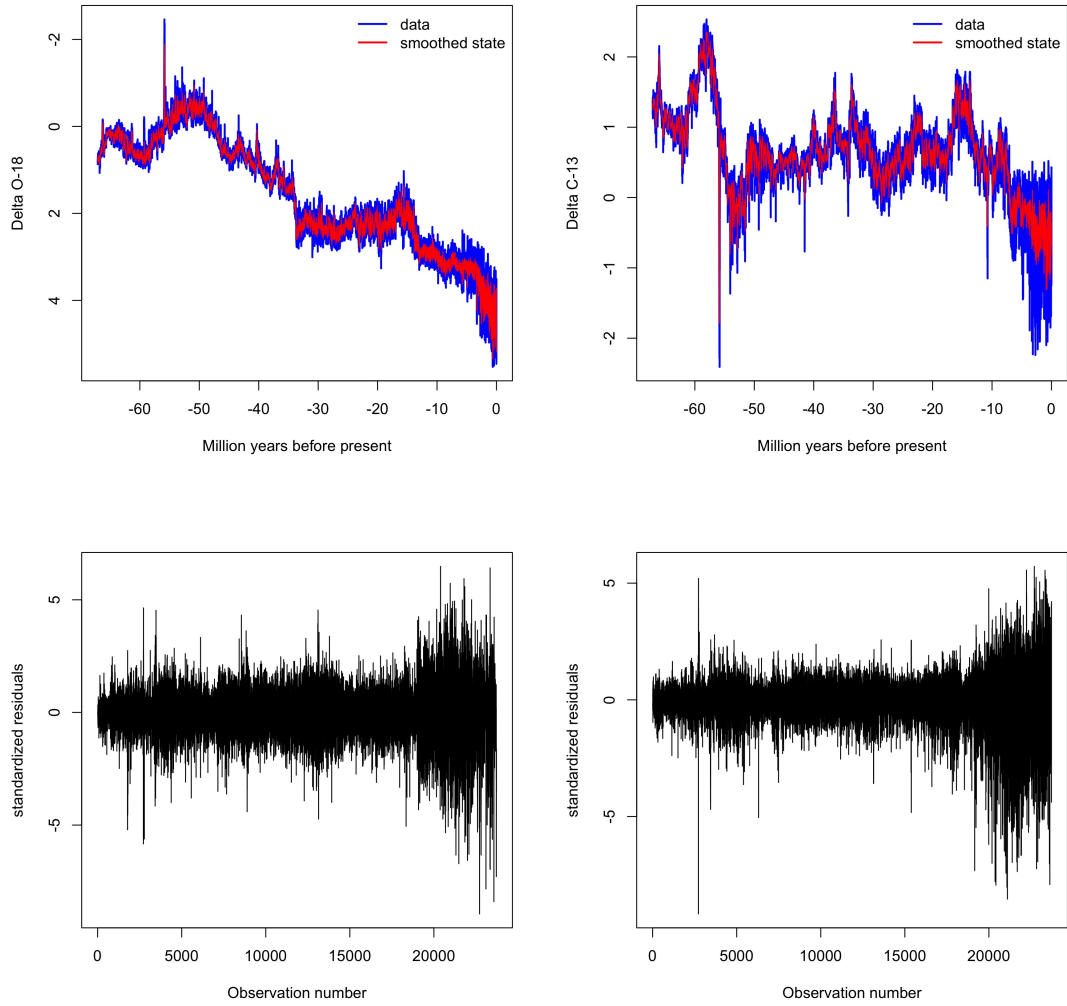


Figure 2: Top left panel:  $\delta^{18}\text{O}$  data (blue) and smoothed state  $\mathbb{E}[\mu_{t+\Delta t} | \{y_s, s \leq \sum \Delta t\}]$  (red) according to model (1) from Kalman smoothing recursions. Top right panel: same for  $\delta^{13}\text{C}$ . Note that the  $y$ -axis for  $\delta^{18}\text{O}$  is reversed, following common practice. Bottom left panel: standardized residuals for  $\delta^{18}\text{O}$ , bottom right panel: standardized residuals for  $\delta^{13}\text{C}$ .

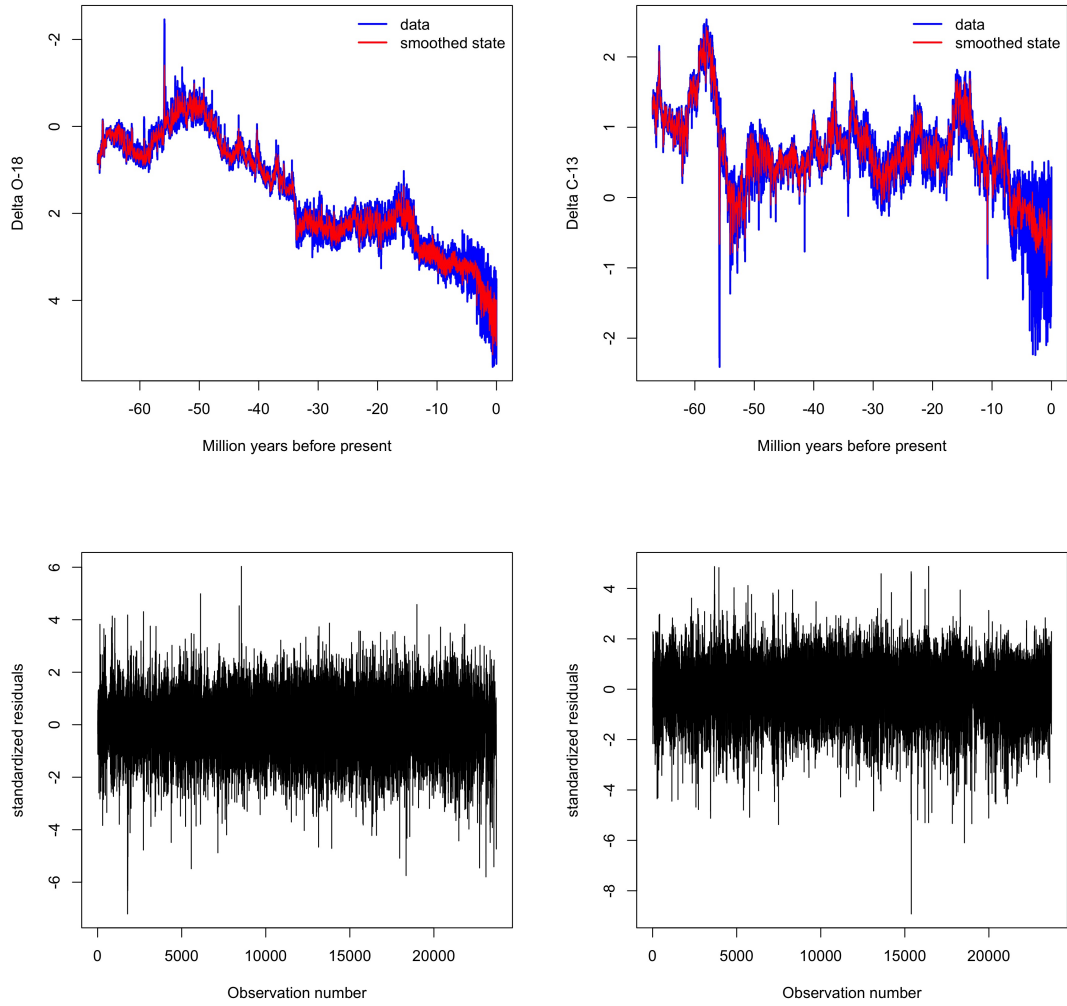


Figure 3: Top left panel:  $\delta^{18}\text{O}$  data (blue) and smoothed state  $\mathbb{E}[\mu_{t+\Delta t} | \{y_s, s \leq \sum \Delta t\}]$  (red) according to model (2) from Kalman smoothing recursions. Top right panel: same for  $\delta^{13}\text{C}$ . Note that the  $y$ -axis for  $\delta^{18}\text{O}$  is reversed, following common practice. Bottom left panel: standardized residuals for  $\delta^{18}\text{O}$ , bottom right panel: standardized residuals for  $\delta^{13}\text{C}$ .

Figure 3, top row, shows the data and the smoothed values of  $\mu_t$  from the Kalman recursions. The bottom row shows the standardized prediction residuals, which appear to have less time variation in the variance in comparison with Figure 2. Table 3 reports the maximum likelihood estimates. The fit as measured by the log-likelihood improves substantially compared with model (1). The same holds for the BIC, despite the much higher number of parameters.

A pattern is apparent that the measurement equation variance decreases with year of publication of the study. A linear regression of the maximum likelihood estimates of the study variances for the  $\delta^{18}\text{O}$  series on the year of publication and a constant yields a highly significantly negative slope estimate of about -0.001 per year. The adjusted coefficient of determination of the regression is 22%, and the F-test of the regression has a  $p$ -value of 0.002. The study coded as “McCarren et al. 2008” in the data file is a bit of an outlier. Excluding this study and its estimated variance from the regression yields an even more highly significant slope estimate of about the same size and an adjusted coefficient of determination of 35%. The same regression for the estimated variances from the  $\delta^{13}\text{C}$  series yields a highly significantly negative slope estimate of -0.004, an adjusted coefficient of determination of 18%, and an F-test of the regression with  $p$ -value 0.007. Excluding the “McCarren et al. 2008” study yields a highly significant slope estimate of -0.0035, an adjusted coefficient of determination of 45%, and an F-test of the regression with  $p$ -value 0.00001.

An alternative specification that takes the different origins of the data into account differentiates the variances in the measurement equation according to benthic foraminifera species. There are 23 distinct species listed in column I (“benthic Species”) of the data file accompanying Westerhold et al. (2020). Therefore, we can modify the measurement equation as follows:

$$y_{i,t} = \mu_t + \varepsilon_{i,t}, \quad \varepsilon_{i,t} \stackrel{i.i.d.}{\sim} \mathbf{N}(0, \sigma_{\varepsilon,i}^2), \quad i = 1, \dots, 23, \quad (3)$$

where  $i$  now indicates the different species of benthic foraminifera. In the appendix, we report graphs of the smoothed signal and maximum likelihood estimates. They show that judging both by the maximized log-likelihood value and by visual inspection of the standardized prediction residuals, the specification that differentiates by studies is superior to this one.

## 2.2 Differentiating transition equation variances according to climate states

Westerhold et al. (2020) identify six different climate states in the records of  $\delta^{18}\text{O}$  and  $\delta^{13}\text{C}$  with the help of recurrence analysis. The periods are shown in Table 4.

We employ these periods to differentiate the variances driving the unobserved component  $\mu_t$  according to climate states. For example, the data plots show that the variance of the observations seem to increase towards the later part of the sample. This is particularly conspicuous for the “icehouse” regime in the  $\delta^{13}\text{C}$  record. A priori, it is not clear whether such a differentiation of the variances should be placed into the measurement or the transition equation. We opt for the transition equation, for two reasons: (1) we already differentiate for originating studies in the measurement equation and want to avoid having to interact these two differentiating dimensions there, and (2) the periods refer to climate states, and we aim for the unobserved component  $\mu_t$  to have a physical interpretation as a climate state variable that is observed in  $y_t$  with measurement noise. Therefore, it seems reasonable to let  $\mu_t$  undergo the variance shifts according to climate states.

The transition equation in model (1) then becomes the following.

$$\mu_{t+\Delta t} = \mu_t + \eta_t, \quad \eta_t \stackrel{i.i.d.}{\sim} \mathbf{N}(0, \sigma_{\eta,j}^2 \Delta t), \quad j \in \{1, \dots, 6\}, \quad (4)$$

where  $j \in \{1, \dots, 6\}$  refers to the six climate state regimes shown in Table 4. The measurement equation (2) is employed, so that the model also differentiates the studies of origin in the measurement variances.

Table 3: Maximum likelihood estimates of model (2). Standard errors in parentheses. “Source” refers to the entry in column “benthic Source” in tab “Table S33” of the data file `aba6853_tables_s8_s34.xlsx` of Westerhold et al. (2020). The identifier “McCarren et al. 2008 et al. 2008” was merged with “McCarren et al. 2008” and “Bickert et al.1997” with “Bickert et al. 1997”. The study Westerhold et al. 2020 is coded in the data file as “this study”. BIC: Bayes information criterion.

Source	No. obs.	$\delta^{18}\text{O}$	No. obs.	$\delta^{13}\text{C}$
$\sigma_{\varepsilon,i}^2$				
“Barnet et al. 2017”	548	0.0015 (0.0002)	548	0.0037 (0.0004)
“Hull et al. 2020”	29	0.0136 (0.0039)	29	0.0136 (0.0040)
“Barnet et al. 2019”	879	0.0053 (0.0004)	879	0.0030 (0.0003)
“Littler et al. 2014”	2164	0.0095 (0.0004)	2164	0.0066 (0.0003)
“McCarren et al. 2008”	47	0.1064 (0.0314)	47	0.3525 (0.0969)
“Lauretano et al. 2015”	636	0.0343 (0.0025)	636	0.0207 (0.0014)
“Stap et al. 2010”	372	0.0305 (0.0025)	372	0.0274 (0.0023)
“Thomas et al. 2018”	86	0.0159 (0.0028)	86	0.0203 (0.0035)
“Lauretano et al. 2016; 2018”	541	0.0072 (0.0007)	541	0.0113 (0.0010)
“Sexton et al. 2011”	301	0.0124 (0.0016)	301	0.0164 (0.0019)
Westerhold et al. 2020	1723	0.0072 (0.0004)	1723	0.0047 (0.0003)
“Westerhold et al. 2018 LLTM”	30	0.0132 (0.0045)	30	0.0575 (0.0182)
“Boscolo Galazzo et al. 2014”	34	0.0227 (0.0065)	34	0.0140 (0.0041)
“Lear et al. 2004”	182	0.0072 (0.0013)	182	0.0069 (0.0012)
“Coxall et al. 2005”	831	0.0089 (0.0006)	831	0.0091 (0.0006)
“Coxall & Wilson, 2011”	413	0.0195 (0.0017)	413	0.0115 (0.0010)
“Riesselmann et al. 2007”	43	0.0161 (0.0046)	43	0.0354 (0.0092)
“Paelike2006 PI Herrle”	258	0.0211 (0.0023)	258	0.0135 (0.0016)
“Wade and Paelike 2004”	152	0.0432 (0.0058)	152	0.0326 (0.0047)
“Liebrand et al. 2011;2016”	3251	0.0114 (0.0004)	3251	0.0107 (0.0003)
“Holbourn et al. 2015”	892	0.0207 (0.0014)	892	0.0107 (0.0007)
“Tian et al. 2014”	61	0.0461 (0.0096)	61	0.0283 (0.0061)
“Holbourn et al. 2014”	1370	0.0144 (0.0007)	1370	0.0086 (0.0005)
“Holbourn et al. 2007;2013;2018”	1987	0.0064 (0.0003)	1987	0.0076 (0.0003)
“Drury et al. 2017”	1129	0.0084 (0.0005)	1129	0.0183 (0.0009)
“Tian et al. 2018”	551	0.0110 (0.0009)	551	0.0276 (0.0019)
UniCambridge Hodell / Westerhold et al. 2020	547	0.0152 (0.0011)	547	0.0109 (0.0008)
“Bell et al. 2014”	260	0.0072 (0.0008)	260	0.0169 (0.0017)
MARUM Bremen / Westerhold et al. 2020	45	0.0092 (0.0021)	45	0.0129 (0.0029)
“Franz & Tiedemann2002”	1304	0.0648 (0.0027)	1050	0.1204 (0.0057)
“Tiedemann & Franz 1997”	330	0.0353 (0.0032)	264	0.0595 (0.0062)
“Billups et al. 1998”	538	0.0313 (0.0022)	538	0.0614 (0.0041)
“Bickert et al. 1997”	2562	0.0611 (0.0022)	2562	0.1561 (0.0047)
“deMenocal et al. 1997”	163	0.0265 (0.0035)	163	0.1398 (0.0169)
$\sigma_{\eta}^2$		1.6235 (0.0506)		1.1547 (0.0368)
log-likelihood	24259	10036.92	23939	9750.60
BIC		-19719.83		-19150.07

Table 4: Climate states identified in Westerhold et al. (2020).

Million Years Ago	Climate State	Obs (unique time stamp)	Obs (data file)
67.10113 to 56	Warmhouse 2	1–2690	21561–24321
56 to 47	Hothouse	2691–5693	18531–21560
47 to 34	Warmhouse 1	5694–7471	16744–18530
34 to 13.9	Coolhouse 1	7472–13933	10067–16743
13.9 to 3.3	Coolhouse 2	13934–20179	3762–10066
3.3 to 0.000564	Icehouse	20180–23722	1–3761



Table 5: Maximum likelihood estimates of model (4). Standard errors in parentheses. “Source” refers to the entry in column “benthic Source” in tab “Table S33” of the data file `aba6853_tables_s8_s34.xlsx` of Westerhold et al. (2020). The identifier “McCarren et al. 2008 et al. 2008” was merged with “McCarren et al. 2008” and “Bickert et al.1997” with “Bickert et al. 1997”. The study Westerhold et al. 2020 is coded in the data file as “this study”. BIC: Bayes information criterion.

Source	No. obs.	$\delta^{18}\text{O}$	No. obs.	$\delta^{13}\text{C}$
$\sigma_{\varepsilon,i}^2$				
“Barnet et al. 2017”	548	0.0031 (0.0003)	548	0.0049 (0.0004)
“Hull et al. 2020”	29	0.0127 (0.0035)	29	0.0126 (0.0037)
“Barnet et al. 2019”	879	0.0080 (0.0005)	879	0.0037 (0.0003)
“Littler et al. 2014”	2164	0.0117 (0.0005)	2164	0.0068 (0.0003)
“McCarren et al. 2008”	47	0.1707 (0.0518)	47	0.1702 (0.0640)
“Lauretano et al. 2015”	636	0.0315 (0.0023)	636	0.0200 (0.0014)
“Stap et al. 2010”	372	0.0308 (0.0024)	372	0.0261 (0.0023)
“Thomas et al. 2018”	86	0.0170 (0.0029)	86	0.0189 (0.0033)
“Lauretano et al. 2016; 2018”	541	0.0089 (0.0008)	541	0.0086 (0.0009)
“Sexton et al. 2011”	301	0.0154 (0.0018)	301	0.0124 (0.0018)
Westerhold et al. 2020	1723	0.0116 (0.0005)	1723	0.0066 (0.0004)
“Westerhold et al. 2018 LLTM”	30	0.0194 (0.0061)	30	0.0758 (0.0227)
“Boscolo Galazzo et al. 2014”	34	0.0243 (0.0063)	34	0.0141 (0.0039)
“Lear et al. 2004”	182	0.0095 (0.0014)	182	0.0081 (0.0013)
“Coxall et al. 2005”	831	0.0094 (0.0006)	831	0.0097 (0.0006)
“Coxall & Wilson, 2011”	413	0.0196 (0.0016)	413	0.0122 (0.0010)
“Riesselmann et al. 2007”	43	0.0188 (0.0043)	43	0.0379 (0.0093)
“Paelike2006 PI Herrle”	258	0.0212 (0.0023)	258	0.0140 (0.0016)
“Wade and Paelike 2004”	152	0.0433 (0.0058)	152	0.0329 (0.0047)
“Liebrand et al. 2011;2016”	3251	0.0116 (0.0004)	3251	0.0112 (0.0004)
“Holbourn et al. 2015”	892	0.0215 (0.0015)	892	0.0119 (0.0008)
“Tian et al. 2014”	61	0.0469 (0.0097)	61	0.0295 (0.0062)
“Holbourn et al. 2014”	1370	0.0147 (0.0008)	1370	0.0091 (0.0005)
“Holbourn et al. 2007;2013;2018”	1987	0.0063 (0.0003)	1987	0.0068 (0.0003)
“Drury et al. 2017”	1129	0.0083 (0.0005)	1129	0.0173 (0.0009)
“Tian et al. 2018”	551	0.0110 (0.0009)	551	0.0269 (0.0019)
UniCambridge Hodell / Westerhold et al. 2020	547	0.0151 (0.0011)	547	0.0105 (0.0008)
“Bell et al. 2014”	260	0.0072 (0.0008)	260	0.0163 (0.0016)
MARUM Bremen / Westerhold et al. 2020	45	0.0092 (0.0021)	45	0.0127 (0.0029)
“Franz & Tiedemann2002”	1304	0.0620 (0.0027)	1050	0.1137 (0.0056)
“Tiedemann & Franz 1997”	330	0.0295 (0.0030)	264	0.0562 (0.0066)
“Billups et al. 1998”	538	0.0313 (0.0022)	538	0.0602 (0.0041)
“Bickert et al. 1997”	2562	0.0395 (0.0014)	2562	0.1280 (0.0041)
“deMenocal et al. 1997”	163	0.0146 (0.0027)	163	0.1020 (0.0135)
$\sigma_{\eta,j}^2$				
67.10113 – 56 MYA (“Warmhouse 2”)	2761	0.3365 (0.0342)	2761	0.6426 (0.0474)
56 – 47 MYA (“Hothouse”)	3030	0.9574 (0.0879)	3030	1.9851 (0.1335)
47 – 34 MYA (“Warmhouse 1”)	1786	0.1608 (0.0242)	1784	0.4026 (0.0438)
34 – 13.9 MYA (“Coolhouse 1”)	6669	1.4655 (0.0859)	6671	0.8437 (0.0569)
13.9 – 3.3 MYA (“Coolhouse 2”)	6282	1.7187 (0.0980)	6139	1.6038 (0.0991)
3.3 – 0.000564 MYA (“Icehouse”)	3731	11.5945 (0.7145)	3554	8.3269 (0.8329)
log-likelihood	24259	10825.05	23939	10038.34
BIC		-21247.13		-19673.73

The maximum likelihood estimates of the resulting model with climate state variances in the transition equation and study variances in the measurement equation are reported in Table 5. It can be seen in comparison with Table 3 that the study variances in the measurement equation are essentially unaffected by the addition of climate-state dependent variances in the transition equation. (The regression of the study variances on the year of publication for  $\delta^{18}\text{O}$  is only significantly negative if the ‘‘McCarren et al. 2008’’ study is excluded. For the  $\delta^{13}\text{C}$  series it remains highly significantly negative throughout.) The climate-state dependent variances vary strongly across the different periods. By far the highest variance is estimated in the ‘‘icehouse’’ period (3.3 to 6e-4 MYA), corresponding to the visual impression of the late record mentioned above. The BIC indicates an additional improvement compared with model (2).

## 2.3 Bivariate random walk plus noise models

The comovement in  $\delta^{18}\text{O}$  and  $\delta^{13}\text{C}$  allows for an improvement of the estimation of the unobserved  $\mu$ -components in  $\delta^{18}\text{O}$  and  $\delta^{13}\text{C}$  by modelling the two time series jointly and estimating the covariance of the error terms  $\eta$ .

To conceptualize the time dependence in the covariances of increments of  $\mu_t^{\delta^{18}\text{O}}$  and  $\mu_t^{\delta^{13}\text{C}}$ , consider two independent Brownian motions  $B_1(t)$  and  $B_3(t)$ . Let

$$B_2(t) = \rho B_1(t) + \sqrt{1 - \rho^2} B_3(t).$$

Here,  $B_1$  stands for the  $\mu$ -component in  $\delta^{18}\text{O}$  and  $B_2$  for the  $\mu$ -component in  $\delta^{13}\text{C}$ . We have for  $s < t$  that

$$\begin{aligned} \text{cov}[B_1(t) - B_1(s), B_2(t) - B_2(s)] &= \mathbb{E}[(B_1(t) - B_1(s))(B_2(t) - B_2(s))] \\ &= \mathbb{E}[(B_1(t) - B_1(s))(\rho(B_1(t) - B_1(s)) + \sqrt{1 - \rho^2}(B_3(t) - B_3(s)))] \\ &= \rho \mathbb{E}[(B_1(t) - B_1(s))^2] = \rho(t - s), \end{aligned}$$

because of the independence of  $B_1$  and  $B_3$ . More generally, for  $s < t < u < v$ ,

$$\begin{aligned} \text{cov}[B_1(v) - B_1(t), B_2(u) - B_2(s)] &= \rho \mathbb{E}[(B_1(v) - B_1(t))(B_1(u) - B_1(s))] \\ &= \rho \mathbb{E} [((B_1(v) - B_1(u)) + (B_1(u) - B_1(t))) ((B_1(u) - B_1(t)) + (B_1(t) - B_1(s)))] \\ &= \rho \mathbb{E} [(B_1(u) - B_1(t))^2] = \rho(u - t), \end{aligned}$$

because

$$\begin{aligned} \mathbb{E}[(B_1(v) - B_1(u))(B_1(u) - B_1(t))] &= \mathbb{E}[(B_1(v) - B_1(u))(B_1(t) - B_1(s))] \\ &= \mathbb{E}[(B_1(u) - B_1(t))(B_1(t) - B_1(s))] = 0. \end{aligned}$$

Thus, the covariance of two increments of  $\mu^{\delta^{18}\text{O}}$  and  $\mu^{\delta^{13}\text{C}}$  is modelled as

$$\mathbb{E}[(\mu_v^{\delta^{18}\text{O}} - \mu_t^{\delta^{18}\text{O}})(\mu_u^{\delta^{13}\text{C}} - \mu_s^{\delta^{13}\text{C}})] = \rho \text{length}((t, v) \cap (s, u)).$$

In all cases in the data, either  $s = t$  or  $u = v$ , and therefore  $\text{length}((t, v) \cap (s, u)) = \min\{v - t, u - s\}$ .

A simple bivariate random walk plus noise model for the two series that extends equation (1) consists of the measurement equations

$$\begin{aligned} y_t^{\delta^{18}\text{O}} &= \mu_t^{\delta^{18}\text{O}} + \varepsilon_t^{\delta^{18}\text{O}}, & \varepsilon_t^{\delta^{18}\text{O}} &\stackrel{i.i.d.}{\sim} \text{N}(0, \sigma_{\varepsilon, \delta^{18}\text{O}}^2), \\ y_t^{\delta^{13}\text{C}} &= \mu_t^{\delta^{13}\text{C}} + \varepsilon_t^{\delta^{13}\text{C}}, & \varepsilon_t^{\delta^{13}\text{C}} &\stackrel{i.i.d.}{\sim} \text{N}(0, \sigma_{\varepsilon, \delta^{13}\text{C}}^2), \end{aligned}$$

Table 6: Maximum likelihood parameter estimates for the simplest bivariate random walk plus noise model. Standard errors in parentheses. BIC: Bayes information criterion.

	$\delta^{18}\text{O}$	$\delta^{13}\text{C}$
$\hat{\sigma}_\eta^2$	1.8154 (0.0475)	1.1991 (0.0396)
$\hat{\sigma}_\varepsilon^2$	0.0205 (0.0002)	0.0341 (0.0004)
$\hat{\rho}$	-0.1700 (0.0209)	
log-likelihood	10229.85	
BIC	-20409.34	

where  $\varepsilon_t^{\delta^{18}\text{O}}$  and  $\varepsilon_t^{\delta^{13}\text{C}}$  are independent. The interesting interaction of the bivariate specification plays out in the covariance matrix of the transition equation, where we allow for correlation of the transition error from the unobserved component in  $\delta^{18}\text{O}$  with the one in  $\delta^{13}\text{C}$ :

$$\begin{aligned}\mu_{t+\Delta t}^{\delta^{18}\text{O}} &= \mu_t^{\delta^{18}\text{O}} + \eta_t^{\delta^{18}\text{O}}, \\ \mu_{t+\Delta t}^{\delta^{13}\text{C}} &= \mu_t^{\delta^{13}\text{C}} + \eta_t^{\delta^{13}\text{C}}.\end{aligned}$$

Collect the state disturbances in the random vector  $\eta_t = (\eta_t^{\delta^{18}\text{O}}, \eta_t^{\delta^{13}\text{C}})^T$ , and assume

$$\eta_t \stackrel{i.i.d.}{\sim} \text{N}(0, Q_t \Delta t), \quad Q_t = \begin{bmatrix} \sigma_{\eta, \delta^{18}\text{O}}^2 & \rho \sigma_{\eta, \delta^{18}\text{O}} \sigma_{\eta, \delta^{13}\text{C}} \\ \rho \sigma_{\eta, \delta^{18}\text{O}} \sigma_{\eta, \delta^{13}\text{C}} & \sigma_{\eta, \delta^{13}\text{C}}^2 \end{bmatrix}. \quad (5)$$

The estimation results of the model are reported in Table 6. The results are qualitatively very close to Table 2. The correlation parameter is estimated at -0.17, and even though the corresponding standard error is much smaller in magnitude, the log-likelihood is close to the sum of the two log-likelihoods from the separate estimation. A plot of the smoothed values and residuals can visually not be distinguished from Figure 2, and so it is omitted here.

We generalize the bivariate approach to distinguish measurement equation variances according to studies and transition equation variances according to climate states in the periods in Table 4. That is, there are six different covariance matrices of the type (5) for the different climate states and 34 study variances for  $\delta^{18}\text{O}$  and  $\delta^{13}\text{C}$ , respectively, for a total of 86 parameters. The system matrices are spelled out in the appendix A.

The correlation of the state disturbances presents itself at a much higher resolution in Table 7 compared to Table 6. There emerges a pattern that high positive correlation in the early record covering warm- and hothouses weakens in the fourth and fifth climate state covering coolhouses and finally reverses sign in the final, icehouse state. Positive correlation in the innovations of two random walks means that there is a tendency that the series move together in local upward or downward runs, and they move in opposite directions in the presence of negative correlation. This pattern was found earlier in Turner (2014), for example. Correlation is substantial in all periods except the fifth, and thus joint modeling of  $\delta^{18}\text{O}$  and  $\delta^{13}\text{C}$  is advantageous in the sense that the estimation of the unobserved states  $\mu_t^{(\delta^{18}\text{O}, \delta^{13}\text{C})}$  can benefit from the larger information set. This is reflected in the log-likelihood of the joint model reported in Table 7, which is substantially higher than the sum of the two separate log-likelihoods in Table 6 (20863.39), at the cost of additional parameters. It is also apparent from a comparison of the estimated variances in the two tables: Almost all measurement equation variances for the different studies are reduced in the joint model compared to the separate estimation, and in the few instances where the variance increased, the difference is not large. (The regression of the study variances on year of publication of the study yields highly significantly negative slope estimates for both proxy series.) On the other hand, the variances of the transition equation for the different climate states are higher for the first five periods in the joint model compared to the separate models, meaning that more variation in the data is captured by the unobserved component of

Table 7: Maximum likelihood estimates of model (5). Standard errors in parentheses. “Source” refers to the entry in column “benthic Source” in tab “Table S33” of the data file `aba6853.tables_s8.s34.xlsx` of Westerhold et al. (2020). The identifier “McCarren et al. 2008 et al. 2008” was merged with “McCarren et al. 2008” and “Bickert et al.1997” with “Bickert et al. 1997”. The study Westerhold et al. 2020 is coded in the data file as “this study”. BIC: Bayes information criterion.

Source	No. obs.	$\delta^{18}\text{O}$	No. obs.	$\delta^{13}\text{C}$
$\sigma_{\varepsilon,i}^2$				
“Barnet et al. 2017”	548	0.0026 (0.0002)	548	0.0043 (0.0004)
“Hull et al. 2020”	29	0.0137 (0.0038)	29	0.0139 (0.0040)
“Barnet et al. 2019”	879	0.0066 (0.0004)	879	0.0029 (0.0002)
“Littler et al. 2014”	2164	0.0096 (0.0004)	2164	0.0054 (0.0003)
“McCarren et al. 2008”	47	0.0611 (0.0139)	47	0.0783 (0.0195)
“Lauretano et al. 2015”	636	0.0298 (0.0022)	636	0.0184 (0.0013)
“Stap et al. 2010”	372	0.0289 (0.0023)	372	0.0257 (0.0022)
“Thomas et al. 2018”	86	0.0134 (0.0023)	86	0.0148 (0.0027)
“Lauretano et al. 2016; 2018”	541	0.0053 (0.0005)	541	0.0048 (0.0006)
“Sexton et al. 2011”	301	0.0075 (0.0009)	301	0.0045 (0.0009)
Westerhold et al. 2020	1723	0.0076 (0.0004)	1723	0.0038 (0.0003)
“Westerhold et al. 2018 LLTM”	30	0.0128 (0.0039)	30	0.0499 (0.0146)
“Boscolo Galazzo et al. 2014”	34	0.0242 (0.0064)	34	0.0146 (0.0041)
“Lear et al. 2004”	182	0.0083 (0.0013)	182	0.0080 (0.0013)
“Coxall et al. 2005”	831	0.0090 (0.0007)	831	0.0096 (0.0006)
“Coxall & Wilson, 2011”	413	0.0180 (0.0016)	413	0.0114 (0.0010)
“Riesselmann et al. 2007”	43	0.0171 (0.0043)	43	0.0334 (0.0085)
“Paelike2006 PI Herrle”	258	0.0210 (0.0023)	258	0.0133 (0.0015)
“Wade and Paelike 2004”	152	0.0422 (0.0057)	152	0.0318 (0.0046)
“Liebrand et al. 2011;2016”	3251	0.0109 (0.0004)	3251	0.0107 (0.0004)
“Holbourn et al. 2015”	892	0.0180 (0.0013)	892	0.0100 (0.0007)
“Tian et al. 2014”	61	0.0431 (0.0090)	61	0.0264 (0.0057)
“Holbourn et al. 2014”	1370	0.0134 (0.0007)	1370	0.0082 (0.0006)
“Holbourn et al. 2007;2013;2018”	1987	0.0061 (0.0003)	1987	0.0066 (0.0003)
“Drury et al. 2017”	1129	0.0083 (0.0005)	1129	0.0174 (0.0009)
“Tian et al. 2018”	551	0.0109 (0.0009)	551	0.0270 (0.0019)
UniCambridge Hodell / Westerhold et al. 2020	547	0.0150 (0.0011)	547	0.0105 (0.0008)
“Bell et al. 2014”	260	0.0072 (0.0008)	260	0.0162 (0.0016)
MARUM Bremen / Westerhold et al. 2020	45	0.0092 (0.0021)	45	0.0128 (0.0029)
“Franz & Tiedemann2002”	1304	0.0615 (0.0027)	1050	0.1132 (0.0055)
“Tiedemann & Franz 1997”	330	0.0307 (0.0031)	264	0.0591 (0.0066)
“Billups et al. 1998”	538	0.0312 (0.0022)	538	0.0602 (0.0041)
“Bickert et al. 1997”	2562	0.0395 (0.0014)	2562	0.1309 (0.0041)
“deMenocal et al. 1997”	163	0.0148 (0.0027)	163	0.1019 (0.0131)
$\sigma_{\eta,j}$				
67.10113 – 56 MYA (“Warmhouse 2”)	2761	0.5924 (0.0522)	2761	0.9224 (0.0635)
56 – 47 MYA (“Hothouse”)	3030	1.9261 (0.1187)	3030	3.3403 (0.1757)
47 – 34 MYA (“Warmhouse 1”)	1786	0.6984 (0.0724)	1784	0.9711 (0.0829)
34 – 13.9 MYA (“Coolhouse 1”)	6669	1.8470 (0.1086)	6671	1.0720 (0.0722)
13.9 – 3.3 MYA (“Coolhouse 2”)	6282	1.7873 (0.1020)	6139	1.6644 (0.1027)
3.3 – 0.000564 MYA (“Icehouse”)	3731	11.5363 (0.7112)	3554	7.0819 (0.6603)
$\rho$				
67.10113 – 56 MYA (“Warmhouse 2”)		0.8212 (0.0185)		
56 – 47 MYA (“Hothouse”)		0.9580 (0.0051)		
47 – 34 MYA (“Warmhouse 1”)		0.9053 (0.0122)		
34 – 13.9 MYA (“Coolhouse 1”)		0.6043 (0.0253)		
13.9 – 3.3 MYA (“Coolhouse 2”)		0.1278 (0.0365)		
3.3 – 0.000564 MYA (“Icehouse”)		-0.8052 (0.0322)		
log-likelihood		22120.73		
BIC		-43375.08		

interest, the “signal”, and less variation remains in the “noise.” The BIC is more highly negative than the sum of the BICs in Table 5. For these reasons, the joint model (5) reported in Table 7 is the preferred model of this section on random-walk-plus-noise models. Figures 9 to 14 in appendix C show the smoothed values of the unobserved components  $\mu_t^{(\delta^{18}\text{O}, \delta^{13}\text{C})}$ , together with the data, and the standardized prediction residuals for the six different climate states.

### 3 Butterworth filtering in the time domain

The models proposed in the previous section naturally lend themselves to an interpretation where a signal  $\mu_t$  is extracted from observations  $y_t$  and distinguished from noise  $\psi_t$ . In this section, we present the well-known connection to signal extraction in the frequency domain and show how the random-walk-plus-noise models of the previous section and the integrated-random-walk-plus-noise models of the next section are time-domain counterparts of the Butterworth filter.

Consider a time series that consists of an autoregressive component  $\mu_t = \phi_1\mu_{t-1} + \dots + \phi_p\mu_{t-p} + \eta_t$ , where  $\eta_t$  is white noise with mean zero and variance  $\sigma_\eta^2$ , plus a white noise contamination  $\varepsilon_t$  with mean zero and variance  $\sigma_\varepsilon^2$  that is independent of  $\eta_t$ :

$$y_t = \Phi^{-1}(L)\eta_t + \varepsilon_t, \quad (6)$$

where  $\Phi(L) = 1 - \phi_1L - \dots - \phi_pL^p$  is the lag polynomial corresponding to the autoregressive component with roots outside the unit circle. For a zero-mean stationary time series such as this, define the autocovariance-generating function

$$g_y(z) = \sum_{j=-\infty}^{\infty} \gamma(j)z^j, \quad z \in \mathbb{C},$$

with  $\gamma(j) = \mathbb{E}(y_t y_{t-j})$ . Since  $\eta_t, \varepsilon_t$  independent, we have that

$$g_y(z) = g_\mu(z) + g_\varepsilon(z),$$

where

$$g_\mu(z) = \frac{\sigma_\eta^2}{|\Phi(z)|^2} = \frac{\sigma_\eta^2}{\Phi(z)\Phi(z^{-1})},$$

and  $g_\varepsilon(z) = \sigma_\varepsilon^2$ . The convention  $|\Phi(z)|^2 = \Phi(z)\Phi(z^{-1})$  is motivated by the fact that we consider  $z \in \mathbb{C}$  only on the unit circle, i.e.,  $z = \exp(-i\lambda)$ ,  $\lambda \in \mathbb{R}$ , and all  $\gamma(j) \in \mathbb{R}$ , thus  $|g(z)|^2 = g(z)\overline{g(z)} = g(z)g(\bar{z})$ , cf. Whittle (1983), p. 12.

The Wiener-Kolmogorov filter for the doubly-infinite sample for model (6) is given by

$$\hat{\mu}_t = \sum_{j=-\infty}^{\infty} b_j y_{t-j} = B(L)y_t,$$

with response function

$$B(z) = \frac{g_\mu(z)}{g_\mu(z) + g_\varepsilon(z)} = \frac{1}{1 + q^{-1}|\Phi(z)|^2},$$

where  $q = \sigma_\eta^2/\sigma_\varepsilon^2$  is the signal-to-noise ratio. For the AR(1) case  $\Phi(z) = 1 - \phi z$ , and  $\phi \rightarrow 1$ , we get the random walk plus noise model

$$y_t = \sum_{j=-\infty}^t \eta_j + \varepsilon_t = (1 - L)^{-1}\eta_t + \varepsilon_t.$$

Bell (1984) showed that the Wiener-Kolmogorov filter is asymptotically valid in the nonstationary case under standard assumptions, see also Gómez (1999). The random walk plus noise model therefore has response function

$$B(z) = \frac{1}{1 + q_1^{-1}|1 - z|^2}.$$

The signal-to-noise ratios  $q_m$  depend on the integration order  $m$  in a manner that is explained below. The integrated random walk plus noise model

$$y_t = \sum_{s=-\infty}^t \sum_{j=-\infty}^s \eta_j + \varepsilon_t = (1 - L)^{-2} \eta_t + \varepsilon_t.$$

has response function

$$B(z) = \frac{1}{1 + q_2^{-1}|1 - z|^4}.$$

Integrating the random walk  $m$  times yields

$$y_t = (1 - L)^{-m} \eta_t + \varepsilon_t$$

with response function

$$B(z) = \frac{1}{1 + q_m^{-1}|1 - z|^{2m}}.$$

For  $z = e^{-i\lambda}$ , we then obtain as the gain function  $G(\lambda)$  of the  $m$ -th order integrated random walk plus noise model

$$G(\lambda) = |B(e^{-i\lambda})| = \frac{1}{1 + q_m^{-1}[(1 - e^{-i\lambda})(1 - e^{i\lambda})]^m}.$$

Since the filter is symmetric, and the response function is non-negative, the gain function is equal to the response function. With  $(1 - e^{-i\lambda})(1 - e^{i\lambda}) = 4 \sin^2(\lambda/2)$ , we have that

$$G(\lambda) = \frac{1}{1 + q_m^{-1} 2^{2m} \sin^{2m}(\lambda/2)}, \quad (7)$$

and, if  $q_m \leq 2^{2m}$ , letting

$$\lambda_h := 2 \sin^{-1} \left( \frac{q_m^{-1/2m}}{2} \right), \quad (8)$$

we can write

$$G(\lambda) = \frac{1}{1 + \left( \frac{\sin \frac{\lambda}{2}}{\sin \frac{\lambda_h}{2}} \right)^{2m}}.$$

This is the gain function of the Butterworth filter of order  $m$  with cutoff frequency  $\lambda_h/2$ , see Harvey and Koopman (2000); Harvey and Trimbur (2003). Estimating the  $m$ -th order integrated random walk plus noise model by maximum likelihood and obtaining variance estimates  $\hat{\sigma}_\eta^2$  and  $\hat{\sigma}_\varepsilon^2$  thus implies an estimated cutoff frequency

$$\frac{\hat{\lambda}_h}{2} = \sin^{-1} \left( \frac{\hat{q}_m^{-1/2m}}{2} \right).$$

The higher the order  $m$  of the filter, the smoother the filtered signal  $\hat{\mu}_t$ , the smaller the estimated variance  $\hat{\sigma}_\eta^2$  relative to  $\hat{\sigma}_\varepsilon^2$  and the lower the estimated signal-to-noise ratio  $\hat{q}_m$ . In this sense,  $q_m$  depends on  $m$ .

## 4 Integrated random walk plus noise models

### 4.1 Specifications

The insights of the last section into the connection of integrated random walk models ( $m > 1$ ) with the Butterworth filter suggest considering models  $y_t = \mu_t + \varepsilon_t$ ,  $\varepsilon \stackrel{i.i.d.}{\sim} \mathbf{N}(0, \sigma_\varepsilon^2)$ , where, for example,  $m = 2$  and

$$\mu_{t_\nu} = \sum_{i_1=1}^{\nu-2} \sum_{i_2=1}^{i_1} \eta_{t_{i_2}}, \quad \eta_{t_\nu} \stackrel{i.i.d.}{\sim} \mathbf{N}(0, \sigma_{\eta,2}^2 \Delta t_\nu).$$

These models smooth the data to a higher degree than the random walk plus noise model ( $m = 1$ ), since the filter weighs lower frequencies more with increasing  $m$ . Let

$$\mu_{t_\nu}^{(1)} = \sum_{i_1=1}^{\nu-1} \eta_{t_{i_1}} = \sum_{i_1=1}^{\nu-2} \eta_{t_{i_1}} + \eta_{t_{\nu-1}} = \mu_{t_{\nu-1}}^{(1)} + \eta_{t_{\nu-1}},$$

then

$$\mu_{t_\nu} = \sum_{i_1=1}^{\nu-3} \sum_{i_2=1}^{i_1} \eta_{t_{i_2}} + \sum_{i_1=1}^{\nu-2} \eta_{t_{i_1}} = \mu_{t_{\nu-1}} + \mu_{t_{\nu-1}}^{(1)}.$$

Then, the transition equation of a corresponding state space model is specified as

$$\begin{bmatrix} \mu_{t+\Delta t} \\ \mu_{t+\Delta t}^{(1)} \end{bmatrix} = \begin{bmatrix} 1 & 1 \\ 0 & 1 \end{bmatrix} \begin{bmatrix} \mu_t \\ \mu_t^{(1)} \end{bmatrix} + \begin{bmatrix} 0 \\ \eta_t \end{bmatrix}, \quad \eta_t \stackrel{i.i.d.}{\sim} \mathbf{N}(0, \sigma_{\eta,2}^2 \Delta t). \quad (9)$$

The measurement equation is as before

$$y_t = \mu_t + \varepsilon_t, \quad \varepsilon \stackrel{i.i.d.}{\sim} \mathbf{N}(0, \sigma_\varepsilon^2),$$

and the distinctions according to studies in the measurement equation and according to periods in the transition equation can be introduced as outlined in Section 2. Appendix A spells out the system matrices.

For  $m = 3$ , let

$$\mu_{t_\nu}^{(1)} = \sum_{i_1=1}^{\nu-1} \eta_{t_{i_1}}$$

as above, and

$$\mu_{t_\nu}^{(2)} = \sum_{i_1=1}^{\nu-2} \sum_{i_2=1}^{i_1} \eta_{t_{i_2}} = \sum_{i_1=1}^{\nu-3} \sum_{i_2=1}^{i_1} \eta_{t_{i_2}} + \sum_{i_1=1}^{\nu-2} \eta_{t_{i_1}} = \mu_{t_{\nu-1}}^{(2)} + \mu_{t_{\nu-1}}^{(1)}.$$

Then, let

$$\mu_{t_\nu} = \sum_{i_1=1}^{\nu-3} \sum_{i_2=1}^{i_1} \sum_{i_3=1}^{i_2} \eta_{t_{i_3}} = \sum_{i_1=1}^{\nu-4} \sum_{i_2=1}^{i_1} \sum_{i_3=1}^{i_2} \eta_{t_{i_3}} + \sum_{i_1=1}^{\nu-3} \sum_{i_2=1}^{i_1} \eta_{t_{i_2}} = \mu_{t_{\nu-1}} + \mu_{t_{\nu-1}}^{(2)}.$$

The transition equation of the corresponding state space model is specified as

$$\begin{bmatrix} \mu_{t+\Delta t} \\ \mu_{t+\Delta t}^{(2)} \\ \mu_{t+\Delta t}^{(1)} \\ \mu_{t+\Delta t}^{(1)} \end{bmatrix} = \begin{bmatrix} 1 & 1 & 0 \\ 0 & 1 & 1 \\ 0 & 0 & 1 \end{bmatrix} \begin{bmatrix} \mu_t \\ \mu_t^{(2)} \\ \mu_t^{(1)} \end{bmatrix} + \begin{bmatrix} 0 \\ 0 \\ \eta_t \end{bmatrix}, \quad \eta_t \stackrel{i.i.d.}{\sim} \mathbf{N}(0, \sigma_{\eta,3}^2 \Delta t). \quad (10)$$

For general  $m$ , let

$$\mu_{t_\nu} = \sum_{i_1=1}^{\nu-m} \sum_{i_2=1}^{i_1} \cdots \sum_{i_m=1}^{i_{m-1}} \eta_{t_{i_m}},$$

and for  $j = 1, \dots, m-1$ , define

$$\mu_{t_\nu}^{(j)} = \sum_{i_1=1}^{\nu-j} \sum_{i_2=1}^{i_1} \cdots \sum_{i_j=1}^{i_{j-1}} \eta_{t_{i_j}} = \mu_{t_{\nu-1}}^{(j)} + \mu_{t_{\nu-1}}^{(j-1)}$$

and thus

$$\mu_{t_\nu} = \mu_{t_{\nu-1}} + \mu_{t_{\nu-1}}^{(m-1)}.$$

The transition equation of the state space model is

$$\begin{bmatrix} \mu_{t+\Delta t} \\ \mu_{t+\Delta t}^{(m-1)} \\ \vdots \\ \mu_{t+\Delta t}^{(2)} \\ \mu_{t+\Delta t}^{(1)} \end{bmatrix} = \begin{bmatrix} 1 & 1 & 0 & 0 & \cdots & 0 & 0 \\ 0 & 1 & 1 & 0 & \cdots & 0 & 0 \\ \vdots & \vdots & \vdots & \vdots & \ddots & \vdots & \vdots \\ 0 & 0 & 0 & 0 & \cdots & 1 & 1 \\ 0 & 0 & 0 & 0 & \cdots & 0 & 1 \end{bmatrix} \begin{bmatrix} \mu_t \\ \mu_t^{(m-1)} \\ \vdots \\ \mu_t^{(2)} \\ \mu_t^{(1)} \end{bmatrix} + \begin{bmatrix} 0 \\ 0 \\ \vdots \\ 0 \\ \eta_t \end{bmatrix}, \quad \eta_t \stackrel{i.i.d.}{\sim} \mathbf{N}(0, \sigma_{\eta,m}^2 \Delta t). \quad (11)$$

## 4.2 Applications

We pursue this class of models in the application to  $\delta^{18}\text{O}$  and  $\delta^{13}\text{C}$  in two ways: First, in order to study the gain functions and the extent of smoothing that the different orders of integration imply, we estimate a single measurement equation variance and a single transition equation variance for  $m = 1, \dots, 6$ . Second, we differentiate measurement equation variances according to studies and transition equation variances according to climate states.

In the constant-variances case, the signal-to-noise ratios are computed as

$$\hat{q}_m = \frac{\hat{\sigma}_{\eta,m}^2 \overline{\Delta t}}{\hat{\sigma}_\varepsilon^2}, \quad (12)$$

where  $\overline{\Delta t}$  is the average time increment per observation from the entire sample. Loosely speaking, the transition equation variance  $\sigma_{\eta,m}^2$  has continuous-time dimension, whereas the measurement equation variance  $\sigma_\varepsilon^2$  has per-observation dimension. Multiplying the transition equation variance by the average time increment per observation makes them dimension-congruent.

Table 8 reports the signal-to-noise ratios computed from Equation (12) and the estimated  $\sigma_{\eta,m}^2$  and  $\sigma_\varepsilon^2$ . (The estimated  $\sigma_\varepsilon^2$  also vary with  $m$ , since greater smoothing in the estimated state leaves more data variance to be captured by the measurement equation, but this is not very important for our analysis, and so we do not index  $\sigma_\varepsilon^2$  with  $m$  in order to keep notation as simple as possible.) The corresponding cutoff frequencies  $\lambda_h$  are computed from Equation (8). Note that the BICs cannot be compared across  $m$ , since  $m$  reflects a design choice of the degree of smoothing, and stronger smoothing implies a deterioration of fit.

Table 8: Estimated signal-to-noise ratios and cutoff frequencies from model (11). BIC: Bayes information criterion.

	$\delta^{18}\text{O}$				$\delta^{13}\text{C}$			
	$\hat{q}_m$	$\hat{\lambda}_h$	log-likelihood	BIC	$\hat{q}_m$	$\hat{\lambda}_h$	log-likelihood	BIC
$m = 1$	0.2537	0.5092	7218.57	-14416.99	0.1009	0.3191	2992.10	-5964.05
$m = 2$	0.0095	0.0974	6237.73	-12455.31	0.0020	0.0445	2204.29	-4388.43
$m = 3$	0.0001	0.0122	4812.72	-9605.40	9.1488e-6	0.0030	1167.39	-2314.64
$m = 4$	2.8447e-7	5.3336e-4	3545.53	-7070.91	2.3601e-8	1.5363e-4	352.74	-685.33
$m = 5$	9.6940e-10	3.1135e-5	2641.94	-5263.72	9.4511e-12	3.0743e-6	-332.63	685.42
$m = 6$	3.0777e-12	1.7543e-6	1820.51	-3620.88	3.5973e-15	5.9978e-8	-836.30	1692.74



The order of integration  $m$  in model (11), equal to the order of the corresponding Butterworth filter, is a design choice by the researcher that reflects the degree of desired smoothing. Given this design choice, the estimation maximizes the log-likelihood of model (11) with respect to  $\sigma_{\eta,m}^2$  and  $\sigma_{\varepsilon}^2$  by way of the Kalman filter recursions (Durbin and Koopman, 2012). Therefore, conditional on the data and  $m$ , the signal-to-noise ratios and the implied gain functions from Equation (7) are optimal in this sense. Table 8 shows that the estimated optimal signal-to-noise ratios decline steeply in  $m$ , which is expected, since a smoother state process  $\mu$  captures less variation in the data, has a smaller variance  $\sigma_{\eta,m}^2$  of the underlying white-noise driver and more variation in the data is captured by  $\sigma_{\varepsilon}^2$ . The maximized log-likelihood decreases sharply in  $m$ . This also reflects the higher degree of smoothing of the estimated latent process  $\mu$  with increasing  $m$ , which makes it increasingly unlikely that the residuals are draws from a normal distribution.

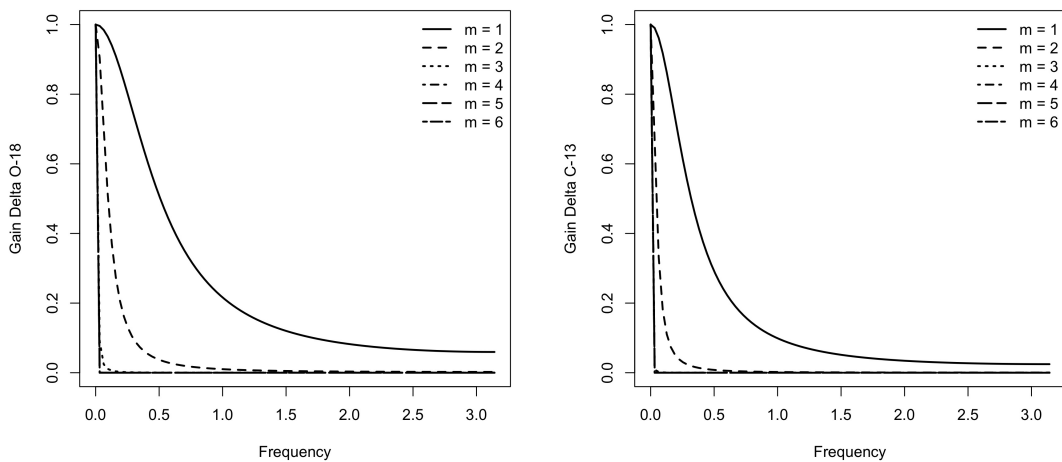


Figure 4: Left panel: Estimated gain functions for  $\delta^{18}\text{O}$  for  $m = 1, \dots, 6$ . Right panel: Same for  $\delta^{13}\text{C}$ .

Figure 4 plots the estimated optimal gain functions for  $\delta^{18}\text{O}$  (left panel) and  $\delta^{13}\text{C}$  (right panel) for different orders  $m$ . The figure and Table 8 show that orders  $m$  beyond 3 result in a cutoff very close to the zero frequency. Nevertheless, the resulting estimated latent processes  $\mu$  still show a good fit and a discernible difference in the degree of smoothing for orders  $m$  between 4 and 6, as we now demonstrate in the estimation that distinguishes measurement equation variances according to studies and transition equation variances according to climate states.

To differentiate measurement equation variances according to studies, we employ the measurement equation specification (2). The transition equation differentiates variances according to climate states as defined in Table 4. We modify Equation (11) such that the last element in the state vector becomes

$$\mu_{t+\Delta t}^{(1)} = \mu_t^{(1)} + \eta_t, \quad \eta_t \stackrel{i.i.d.}{\sim} \text{N}(0, \sigma_{\eta,m,j}^2), \quad j = 1, \dots, 6, \quad m \in \{2, 4, 6, 8\}. \quad (13)$$

Tables 9 and 10 report the estimated measurement equation variances for  $\delta^{18}\text{O}$  and  $\delta^{13}\text{C}$ , respectively. Table 11 reports the estimated transition equation variances. Figures 5 and 6 show the estimated latent state processes  $\mu$  for  $\delta^{18}\text{O}$  and  $\delta^{13}\text{C}$ , respectively, in the left column. The right column in both figures shows the corresponding standardized residuals. Figures 5 and 6 show that there is no visually discernible difference in the estimated latent processes between orders  $m = 6$  and  $m = 8$ . Tables 9 and 10 show that the differences in the estimated measurement equation variances between  $m = 6$  and  $m = 8$  are small and within the variation indicated by the estimated standard errors. Table 11 shows differences in transition equation

Table 9: Maximum likelihood estimates of model (11) for  $\delta^{18}\text{O}$ . Standard errors in parentheses. “Source” refers to the entry in column “benthic Source” in tab “Table S33” of the data file `aba6853_tables_s8_s34.xlsx` of Westerhold et al. (2020). The identifier “McCarren et al. 2008 et al. 2008” was merged with “McCarren et al. 2008” and “Bickert et al.1997” with “Bickert et al. 1997”. The study Westerhold et al. 2020 is coded in the data file as “this study”. BIC: Bayes information criterion.

Source	$m = 2$	$m = 4$	$m = 6$	$m = 8$
$\sigma_{\varepsilon,i}^2$	$\delta^{18}\text{O}$			
“Barnet et al. 2017”	0.0046 (0.0003)	0.0053 (0.0003)	0.0056 (0.0004)	0.0057 (0.0004)
“Hull et al. 2020”	0.0146 (0.0039)	0.0158 (0.0042)	0.0159 (0.0043)	0.0161 (0.0043)
“Barnet et al. 2019”	0.0109 (0.0006)	0.0134 (0.0007)	0.0144 (0.0007)	0.0152 (0.0008)
“Littler et al. 2014”	0.0140 (0.0005)	0.0158 (0.0005)	0.0183 (0.0007)	0.0204 (0.0007)
“McCarren et al. 2008”	0.3357 (0.0727)	0.3843 (0.0811)	0.4849 (0.1011)	0.5193 (0.1079)
“Lauretano et al. 2015”	0.0299 (0.0022)	0.0314 (0.0022)	0.0353 (0.0024)	0.0367 (0.0024)
“Stap et al. 2010”	0.0312 (0.0024)	0.0328 (0.0025)	0.0338 (0.0025)	0.0341 (0.0026)
“Thomas et al. 2018”	0.0189 (0.0031)	0.0229 (0.0037)	0.0304 (0.0048)	0.0293 (0.0045)
“Lauretano et al. 2016; 2018”	0.0161 (0.0011)	0.0207 (0.0013)	0.0246 (0.0015)	0.0258 (0.0016)
“Sexton et al. 2011”	0.0230 (0.0020)	0.0244 (0.0020)	0.0270 (0.0022)	0.0284 (0.0024)
Westerhold et al. 2020	0.0141 (0.0005)	0.0153 (0.0005)	0.0159 (0.0006)	0.0162 (0.0006)
“Westerhold et al. 2018 LLTM”	0.0267 (0.0073)	0.0269 (0.0073)	0.0266 (0.0072)	0.0268 (0.0072)
“Boscolo Galazzo et al. 2014”	0.0286 (0.0072)	0.0337 (0.0084)	0.0350 (0.0087)	0.0362 (0.0090)
“Lear et al. 2004”	0.0163 (0.0019)	0.0236 (0.0026)	0.0247 (0.0027)	0.0255 (0.0027)
“Coxall et al. 2005”	0.0137 (0.0008)	0.0183 (0.0009)	0.0188 (0.0009)	0.0192 (0.0010)
“Coxall & Wilson, 2011”	0.0216 (0.0017)	0.0250 (0.0018)	0.0256 (0.0018)	0.0261 (0.0019)
“Riesselmann et al. 2007”	0.0192 (0.0042)	0.0205 (0.0046)	0.0220 (0.0051)	0.0227 (0.0055)
“Paelike2006 PI Herrle”	0.0248 (0.0024)	0.0305 (0.0027)	0.0309 (0.0028)	0.0315 (0.0028)
“Wade and Paelike 2004”	0.0496 (0.0060)	0.0605 (0.0070)	0.0610 (0.0071)	0.0614 (0.0071)
“Liebrand et al. 2011;2016”	0.0147 (0.0004)	0.0229 (0.0006)	0.0234 (0.0006)	0.0236 (0.0006)
“Holbourn et al. 2015”	0.0324 (0.0017)	0.0502 (0.0025)	0.0522 (0.0026)	0.0539 (0.0027)
“Tian et al. 2014”	0.0573 (0.0110)	0.0988 (0.0181)	0.1009 (0.0184)	0.1014 (0.0185)
“Holbourn et al. 2014”	0.0208 (0.0010)	0.0402 (0.0016)	0.0402 (0.0016)	0.0414 (0.0016)
“Holbourn et al. 2007;2013;2018”	0.0103 (0.0004)	0.0205 (0.0007)	0.0208 (0.0007)	0.0210 (0.0007)
“Drury et al. 2017”	0.0101 (0.0005)	0.0162 (0.0007)	0.0163 (0.0007)	0.0165 (0.0007)
“Tian et al. 2018”	0.0127 (0.0009)	0.0169 (0.0010)	0.0169 (0.0010)	0.0173 (0.0011)
UniCambridge Hodell / Westerhold et al. 2020	0.0176 (0.0012)	0.0260 (0.0016)	0.0261 (0.0016)	0.0263 (0.0016)
“Bell et al. 2014”	0.0081 (0.0008)	0.0147 (0.0013)	0.0149 (0.0013)	0.0154 (0.0014)
MARUM Bremen / Westerhold et al. 2020	0.0093 (0.0020)	0.0155 (0.0033)	0.0155 (0.0033)	0.0158 (0.0033)
“Franz & Tiedemann2002”	0.0643 (0.0027)	0.0690 (0.0028)	0.0702 (0.0028)	0.0727 (0.0029)
“Tiedemann & Franz 1997”	0.0310 (0.0029)	0.0374 (0.0032)	0.0377 (0.0032)	0.0386 (0.0032)
“Billups et al. 1998”	0.0346 (0.0023)	0.0408 (0.0025)	0.0411 (0.0025)	0.0422 (0.0026)
“Bickert et al. 1997”	0.0462 (0.0015)	0.0543 (0.0017)	0.0597 (0.0019)	0.0645 (0.0024)
“deMenocal et al. 1997”	0.0233 (0.0031)	0.0273 (0.0034)	0.0288 (0.0035)	0.0298 (0.0036)
log-likelihood	9265.22	7234.54	6072.71	5033.15
BIC	-18127.47	-14066.12	-11742.45	-9663.34

Table 10: Maximum likelihood estimates of model (11) for  $\delta^{13}\text{C}$ . Standard errors in parentheses. “Source” refers to the entry in column “benthic Source” in tab “Table S33” of the data file `aba6853_tables_s8_s34.xlsx` of Westerhold et al. (2020). The identifier “McCarren et al. 2008 et al. 2008” was merged with “McCarren et al. 2008” and “Bickert et al.1997” with “Bickert et al. 1997”. The study Westerhold et al. 2020 is coded in the data file as “this study”. BIC: Bayes information criterion.

Source	$m = 2$	$m = 4$	$m = 6$	$m = 8$
$\sigma_{\varepsilon,i}^2$	$\delta^{13}\text{C}$			
“Barnet et al. 2017”	0.0073 (0.0005)	0.0083 (0.0005)	0.0097 (0.0006)	0.0102 (0.0006)
“Hull et al. 2020”	0.0117 (0.0033)	0.0113 (0.0031)	0.0120 (0.0032)	0.0127 (0.0034)
“Barnet et al. 2019”	0.0056 (0.0003)	0.0079 (0.0005)	0.0117 (0.0006)	0.0138 (0.0007)
“Littler et al. 2014”	0.0092 (0.0003)	0.0117 (0.0004)	0.0163 (0.0005)	0.0176 (0.0006)
“McCarren et al. 2008”	0.6930 (0.1494)	0.8323 (0.1740)	0.9165 (0.1908)	0.9725 (0.2020)
“Lauretano et al. 2015”	0.0203 (0.0014)	0.0225 (0.0014)	0.0245 (0.0016)	0.0265 (0.0016)
“Stap et al. 2010”	0.0244 (0.0020)	0.0255 (0.0021)	0.0268 (0.0021)	0.0278 (0.0022)
“Thomas et al. 2018”	0.0200 (0.0032)	0.0217 (0.0035)	0.0248 (0.0040)	0.0278 (0.0046)
“Lauretano et al. 2016; 2018”	0.0188 (0.0014)	0.0320 (0.0021)	0.0366 (0.0023)	0.0378 (0.0024)
“Sexton et al. 2011”	0.0249 (0.0023)	0.0316 (0.0027)	0.0325 (0.0027)	0.0331 (0.0028)
Westerhold et al. 2020	0.0109 (0.0004)	0.0130 (0.0005)	0.0147 (0.0005)	0.0174 (0.0006)
“Westerhold et al. 2018 LLTM”	0.0962 (0.0259)	0.0932 (0.0245)	0.0920 (0.0238)	0.1108 (0.0293)
“Boscolo Galazzo et al. 2014”	0.0158 (0.0041)	0.0173 (0.0044)	0.0203 (0.0051)	0.0276 (0.0068)
“Lear et al. 2004”	0.0135 (0.0016)	0.0179 (0.0020)	0.0184 (0.0020)	0.0184 (0.0020)
“Coxall et al. 2005”	0.0131 (0.0007)	0.0167 (0.0008)	0.0171 (0.0009)	0.0172 (0.0009)
“Coxall & Wilson, 2011”	0.0140 (0.0011)	0.0158 (0.0011)	0.0162 (0.0012)	0.0163 (0.0012)
“Riesselmann et al. 2007”	0.0380 (0.0088)	0.0435 (0.0111)	0.0994 (0.0330)	0.1777 (0.0441)
“Paelike2006 PI Herrle”	0.0177 (0.0017)	0.0222 (0.0020)	0.0223 (0.0020)	0.0222 (0.0020)
“Wade and Paelike 2004”	0.0360 (0.0047)	0.0396 (0.0050)	0.0414 (0.0053)	0.0431 (0.0055)
“Liebrand et al. 2011;2016”	0.0138 (0.0004)	0.0178 (0.0005)	0.0183 (0.0005)	0.0185 (0.0005)
“Holbourn et al. 2015”	0.0184 (0.0010)	0.0263 (0.0013)	0.0279 (0.0014)	0.0287 (0.0014)
“Tian et al. 2014”	0.0358 (0.0069)	0.0426 (0.0079)	0.0429 (0.0079)	0.0434 (0.0080)
“Holbourn et al. 2014”	0.0142 (0.0006)	0.0184 (0.0007)	0.0196 (0.0008)	0.0200 (0.0008)
“Holbourn et al. 2007;2013;2018”	0.0112 (0.0004)	0.0159 (0.0006)	0.0200 (0.0007)	0.0231 (0.0009)
“Drury et al. 2017”	0.0201 (0.0010)	0.0299 (0.0013)	0.0326 (0.0014)	0.0332 (0.0014)
“Tian et al. 2018”	0.0290 (0.0019)	0.0373 (0.0023)	0.0413 (0.0025)	0.0425 (0.0026)
UniCambridge Hodel / Westerhold et al. 2020	0.0124 (0.0008)	0.0157 (0.0010)	0.0197 (0.0012)	0.0206 (0.0013)
“Bell et al. 2014”	0.0180 (0.0017)	0.0256 (0.0023)	0.0270 (0.0024)	0.0272 (0.0024)
MARUM Bremen / Westerhold et al. 2020	0.0134 (0.0030)	0.0160 (0.0035)	0.0172 (0.0037)	0.0172 (0.0037)
“Franz & Tiedemann2002”	0.1167 (0.0055)	0.1209 (0.0056)	0.1391 (0.0063)	0.1396 (0.0063)
“Tiedemann & Franz 1997”	0.0608 (0.0064)	0.0631 (0.0064)	0.0744 (0.0071)	0.0748 (0.0072)
“Billups et al. 1998”	0.0641 (0.0042)	0.0698 (0.0044)	0.0711 (0.0044)	0.0712 (0.0044)
“Bickert et al. 1997”	0.1406 (0.0043)	0.1625 (0.0049)	0.2077 (0.0059)	0.2073 (0.0058)
“deMenocal et al. 1997”	0.1175 (0.0145)	0.1364 (0.0163)	0.2215 (0.0252)	0.2201 (0.0249)
log-likelihood	8445.04	6212.34	4982.08	4043.34
BIC	-16487.11	-12021.72	-9561.19	-7683.71

Table 11: Maximum likelihood estimates of model (11). Standard errors in parentheses. LLH: log-likelihood.

$\sigma_{\eta,j}^2$	$\delta^{18}\text{O}$							LLH
Period	1	2	3	4	5	6	LLH	
$m = 2$	0.0034 (0.0007)	0.0107 (0.0019)	0.0007 (0.0002)	0.0425 (0.0049)	0.0824 (0.0094)	0.5175 (0.0493)	9265.22	
$m = 4$	4.6e-8 (1.3e-8)	3.2e-7 (1e-7)	5e-9 (1.7e-9)	3.4e-9 (8.2e-10)	1.2e-12 (6.5e-13)	4.7e-4 (7e-5)	7234.54	
$m = 6$	4.1e-13 (1.8e-13)	4.7e-14 (2.5e-14)	7.4e-14 (2.7e-14)	8.9e-15 (2.3e-15)	2.9e-20 (1.5e-20)	2.8e-7 (5.1e-8)	6072.71	
$m = 8$	2.2e-18 (8.1e-19)	2.2e-21 (8.3e-22)	7.7e-19 (3.8e-19)	2.9e-20 (1.0e-20)	9.7e-30 (4.7e-30)	1.3e-10 (4.1e-11)	5033.15	
	$\delta^{13}\text{C}$							LLH
Period	1	2	3	4	5	6	LLH	
$m = 2$	0.03024 (0.0036)	0.0726 (0.0103)	0.0041 (0.0011)	0.0108 (0.0014)	0.0423 (0.0059)	0.1158 (0.0197)	8445.04	
$m = 4$	1.8e-5 (4.6e-6)	4.8e-6 (1.2e-6)	2.0e-7 (6.2e-8)	7.2e-9 (1.5e-9)	8.1e-8 (2.4e-8)	1.6e-6 (4.6e-7)	6212.34	
$m = 6$	7.1e-12 (2.9e-12)	1.3e-10 (4.7e-11)	6.2e-13 (2.9e-13)	3.0e-14 (6.0e-15)	1.8e-15 (6.1e-16)	6.2e-20 (5.7e-20)	4982.08	
$m = 8$	1.9e-17 (5.4e-18)	3.7e-15 (1.5e-15)	2.3e-20 (1.0e-20)	1.5e-19 (3.2e-20)	5.6e-23 (4.4e-23)	4.1e-27 (2.5e-27)	4043.34	

variances between  $m = 6$  and  $m = 8$  of several orders of magnitude, but in very high decimal places,  $10^{-8}$  being the biggest order that appears.

Between  $m = 4$  and  $m = 6$ , in contrast, there is a visually discernible difference in the estimated latent state processes  $\mu$  for  $\delta^{18}\text{O}$  and  $\delta^{13}\text{C}$ , and the estimated variances, both in measurement and transition equation, differ substantially. We conclude that integration orders up to  $m = 6$  are meaningful for  $\delta^{18}\text{O}$  and  $\delta^{13}\text{C}$ . We recommend using specifications (13) for the transition equation and (2) for the measurement equation, as Tables 9, 10, and 11 show that the differences in the estimated variances are substantial. Comparing log-likelihoods across  $m$ 's is not meaningful, since  $m$  is a design choice. For given  $m$ , however, comparing log-likelihoods in Tables 8 on the one hand and 9 and 10 on the other, reveals that allowing for study- and climate states-dependent variances substantially improves the model fit.

## 5 Imputing regularly time-stamped values

State space models handle missing observations seamlessly, since the Kalman recursions compute the predicted values  $\mathbb{E}[\mu_{t+\Delta t}|\{y_s, s \leq t\}]$ , the filtered values  $\mathbb{E}[\mu_{t+\Delta t}|\{y_s, s \leq t + \Delta t\}]$ , and the smoothed values  $\mathbb{E}[\mu_{t+\Delta t}|\{y_s, s \leq \sum \Delta t\}]$  for all time stamps, also those that have NAs in the  $y_t$  vector in the measurement equation (Durbin and Koopman, 2012). We obtain smoothed estimates  $\mathbb{E}[\mu_{t+\Delta t}|\{y_s, s \leq \sum \Delta t\}]$  of the unobserved component  $\mu$  from any of the models discussed in this paper at an equidistantly spaced grid of time stamps in the following manner.

We define a constant time increment  $\Delta$  (in years) and generate an equidistant partition of the interval  $[-67, 0]$  (MY) at mesh  $\Delta$ . This results in  $N_g = [67000000/\Delta]$  time stamps for which there are no observations (unless by coincidence), and so we fill the corresponding elements in  $y_t$  with ‘‘NA.’’ Here,  $[\cdot]$  denotes the Gauss-bracket. This partition is merged with the irregularly spaced data and ordered according to time stamps, resulting in  $N + N_g = 23722 + [67000000/\Delta]$  time stamps. The maximum likelihood estimate of the parameter vector of the chosen model estimated on the  $N$  available data points is used as input to the Kalman recursions, which are then run on the extended data matrix of  $N + N_g$  rows. The Kalman recursions compute the predicted, filtered, and smoothed values for the  $N + N_g$  observations, and we extract the  $N_g$  regularly time stamped smoothed values.

This state space method of obtaining regularly time stamped values can therefore be seen as an alternative to the nonuniform discrete inverse Fourier transform (Bagchi and Mitra, 1996). The state space method in the time domain has the advantage of allowing for a higher resolution of other features of the data, in our application a differentiation of variances in the measurement equation according to studies or species and in the transition equation according to climate states. It also provides estimates of the variances, and thus signal-to-noise ratios and cutoff frequencies, that are optimal in the maximum likelihood sense. This leaves only the order of integration (order of the filter) to be chosen by the researcher.

Based on both the Bayes information criterion and the log-likelihood of the fitted model, we arrive at a preference for the bivariate random-walk-plus-noise model with measurement equation variances differentiated according to studies of origin and transition equation variances differentiated according to climate states. We therefore use this model to illustrate the imputation of regularly time stamped values via the Kalman smoother, which may be used by researchers in further analyses employing standard time series techniques. Figure 7 shows equispaced time-stamped smoothed values for the unobserved components for  $\delta^{18}\text{O}$  (top row) and  $\delta^{13}\text{C}$  (bottom row) for three different mesh values  $\Delta = (100000, 10000, 1000)$ .

## 6 Conclusion

We specified state space models for the time series of  $\delta^{18}\text{O}$  and  $\delta^{13}\text{C}$  provided in Westerhold et al. (2020). The models addressed the central challenges of the time series: non-stationarity with trends in varying directions, irregular spacing of the time stamps of the observations, multiple observations at certain time stamps, different studies of origin of the data, different climate states covered by the data, and covariation in the two series. The models were specified and estimated by maximum likelihood in the time domain, allowing for a direct interpretation as Butterworth filters in the frequency domain. We showed that accounting for the different studies of origin of the data by way of differentiating measurement equation variances substantially improves the model fit. Another improvement is achieved by differentiating the variances in the state equation by climate states, as they were identified in Westerhold et al. (2020). Bivariate specifications are fruitful in that they use the covariation in the  $\delta^{18}\text{O}$  and  $\delta^{13}\text{C}$  series to inform the estimation of the models. We showed that integration orders of the unobserved component, which at the same time are the orders of the corresponding Butterworth filters, up to six are meaningful for the two time series. They yield visually distinct estimated latent components with different degrees of smoothing. Therefore, the order is a design choice made by the researcher reflecting their preference for a degree of smoothing. Given this choice, and the data, the maximum likelihood estimation yields optimal estimates of the measurement and state equation variances. These correspond to optimal signal-to-noise ratios (and thus cutoff frequencies) for the corresponding Butterworth filters. In summary, well developed statistical theory, both in the time and in the frequency domains, can be employed to specify time series models for  $\delta^{18}\text{O}$  and  $\delta^{13}\text{C}$  that can resolve many of the rich features of these fascinating data. In future research, we will address uncertainty in the time stamps of the observations and relate the  $\delta^{18}\text{O}$  and  $\delta^{13}\text{C}$  measurements to paleo-estimates of atmospheric  $\text{CO}_2$  concentrations.

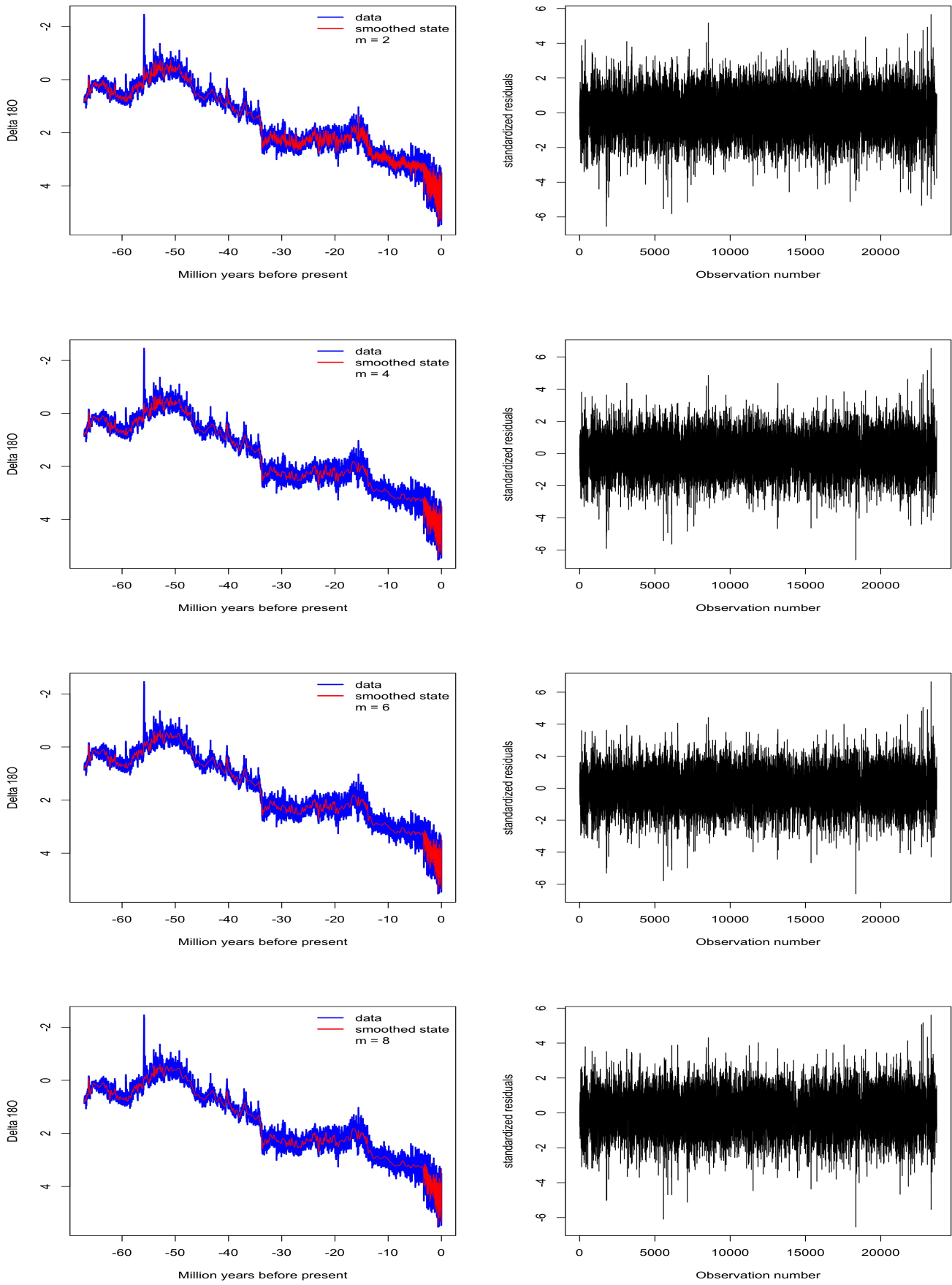


Figure 5: Left column:  $\delta^{18}\text{O}$  data (blue) and smoothed state  $\mathbb{E}[\mu_{t+\Delta t} | \{y_s, s \leq \sum \Delta t\}]$  (red) according to model (11) for  $m = 2, 4, 6, 8$ . Right column: standardized residuals.

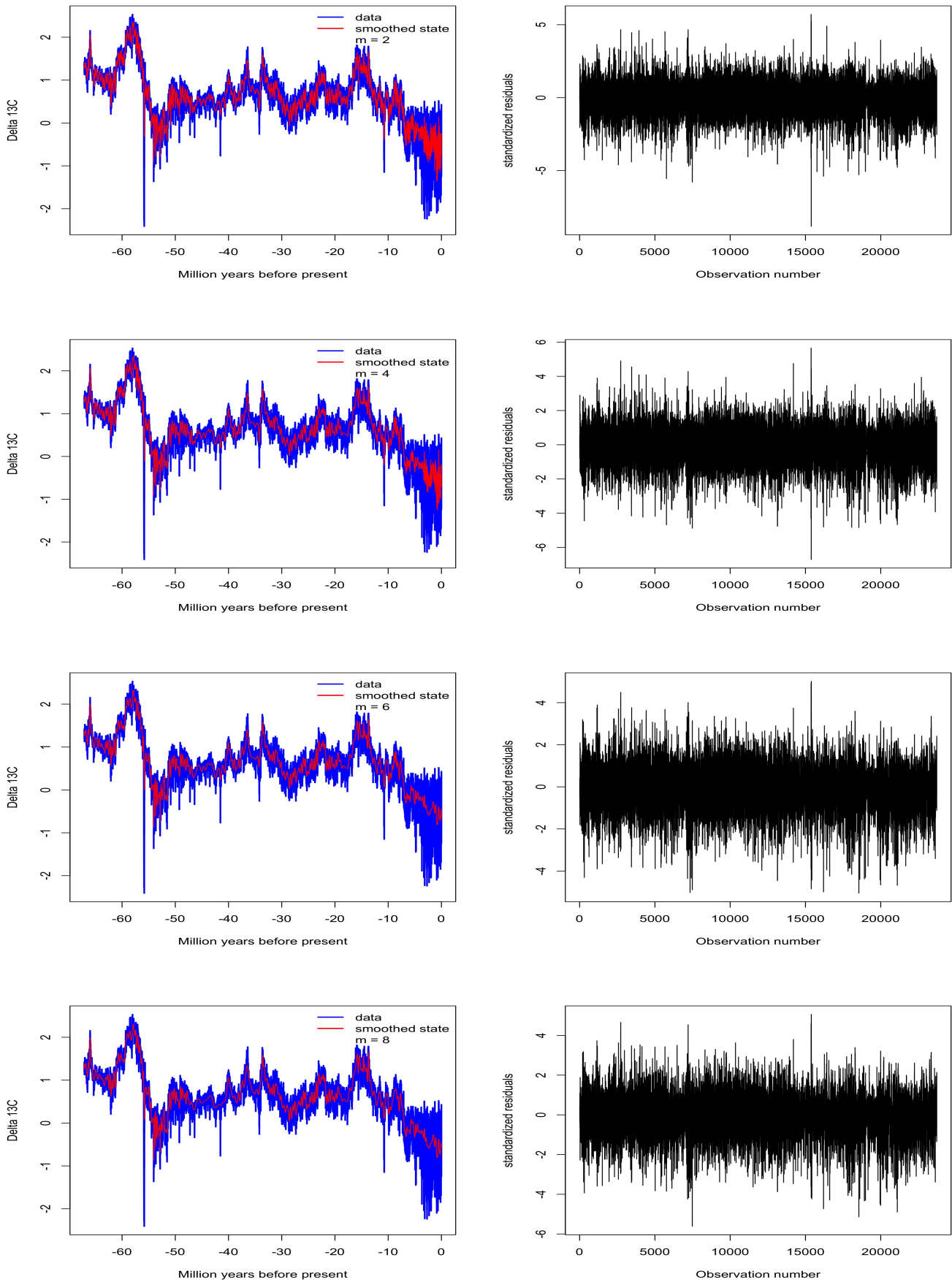


Figure 6: Left column:  $\delta^{13}\text{C}$  data (blue) and smoothed state  $\mathbb{E}[\mu_{t+\Delta t} | \{y_s, s \leq \sum \Delta t\}]$  (red) according to model (11) for  $m = 2, 4, 6, 8$ . Right column: standardized residuals.

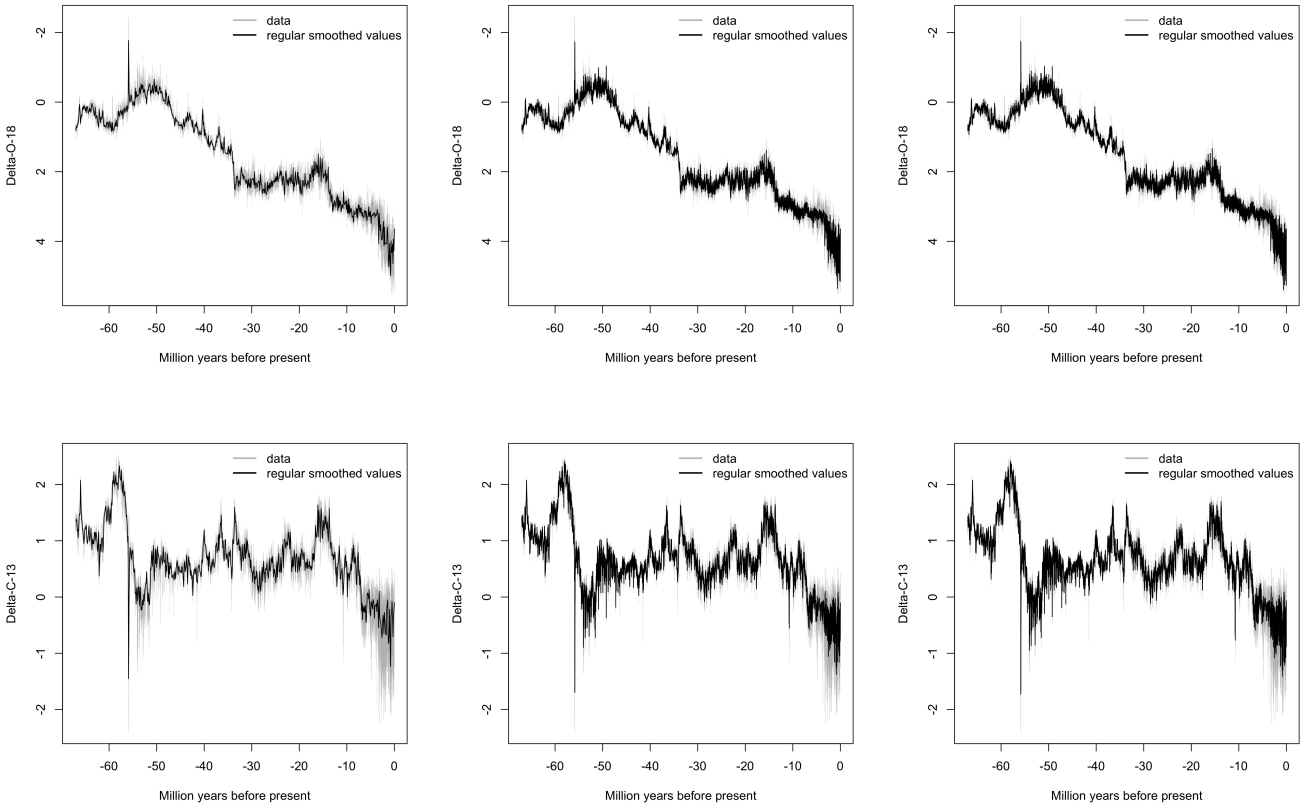


Figure 7: Regularly time-stamped smoothed values from Model (5) with measurement variances according to studies and transition variances according to climate states. Upper row:  $\delta^{18}\text{O}$  with mesh  $\Delta = 100000$  years (left panel),  $\Delta = 10000$  years (middle panel),  $\Delta = 1000$  years (right panel). Bottom row:  $\delta^{13}\text{C}$  with mesh  $\Delta = 100000$  years (left panel),  $\Delta = 10000$  years (middle panel),  $\Delta = 1000$  years (right panel).



# A System matrices of the state space models

## A.1 Univariate random walk plus noise specifications

The measurement equation relates the data points from the data file of Westerhold et al. (2020) to the unobserved components  $\mu_t$  that are the central part of our modeling approach. A fact about the data set that has direct relevance for the dimension chosen for the measurement equation is that there are at most four data points at any given time stamp for each of the two time series, and they can originate from different studies. Denote the data points by  $y$ , the studies by  $i$ , the unobserved components by  $\mu$ , the climate states by  $j$ , and time by  $t$ .

The set of unique time stamps is given by  $t_\nu$ ,  $\nu \in \{1, \dots, N\}$ ,  $N = 23722$ . The time stamps  $t_\nu$  fall into the interval  $[-67.10113, -0.000564]$ , which is read as 67.10113 to 0.000564 million years ago. At time  $t_\nu$ ,

$$\underbrace{\begin{bmatrix} y_{i_1, t_\nu} \\ y_{i_2, t_\nu} \\ y_{i_3, t_\nu} \\ y_{i_4, t_\nu} \end{bmatrix}}_{y_{t_\nu} \in \mathbb{R}^{4 \times 1}} = \underbrace{\begin{bmatrix} 1 \\ 1 \\ 1 \\ 1 \end{bmatrix}}_{Z \in \mathbb{R}^{4 \times 1}} \mu_{t_\nu} + \underbrace{\begin{bmatrix} \varepsilon_{i_1, t_\nu} \\ \varepsilon_{i_2, t_\nu} \\ \varepsilon_{i_3, t_\nu} \\ \varepsilon_{i_4, t_\nu} \end{bmatrix}}_{\varepsilon_{t_\nu} \in \mathbb{R}^{4 \times 1}}, \quad \mu_{t_\nu} \in \mathbb{R}.$$

The index  $i_{\{1,2,3,4\}} \in \{1, \dots, 34\}$  denotes the 34 different studies of origin coded in the data file. The zero-mean measurement equation error vector is assumed to be identically and independently normally distributed:

$$\varepsilon_{t_\nu} \stackrel{i.i.d.}{\sim} \mathbf{N}(0, H_{t_\nu}),$$

with covariance matrix

$$H_{t_\nu} = \text{diag}(\sigma_{\varepsilon, i_1}^2, \sigma_{\varepsilon, i_2}^2, \sigma_{\varepsilon, i_3}^2, \sigma_{\varepsilon, i_4}^2).$$

The relation between  $t_\nu$  and  $i_{(\cdot)}$  is the mapping ‘‘study  $i_{(\cdot)}$  provided the data point  $y_{i_{(\cdot)}, t_\nu}$  for time stamp  $t_\nu$ .’’

The transition equation for the unobserved component is given as follows.

$$\mu_{t_\nu + \Delta t_\nu} = \mu_{t_\nu} + \sqrt{\Delta t_\nu} \eta_{j, t_\nu},$$

where  $j \in \{1, \dots, 6\}$  indicates the six different climate states identified in Westerhold et al. (2020). The zero-mean transition equation error is assumed to be identically and independently normally distributed:  $\eta_{j, t_\nu} \stackrel{i.i.d.}{\sim} \mathbf{N}(0, Q_{t_\nu})$ ,  $Q_{t_\nu} = \sigma_{\eta, j}^2$ . The relation between  $t_\nu$  and  $j$  is the mapping ‘‘time  $t_\nu$  falls into period  $j$  according to Table 4.’’

## A.2 Bivariate random walk plus noise specifications

For the bivariate specifications, let (1) denote  $\delta^{18}\text{O}$  and (2)  $\delta^{13}\text{C}$ .

The measurement equation is given as follows.

$$\underbrace{\begin{bmatrix} y_{i_1, t_\nu}^{\delta^{18}\text{O}} \\ y_{i_2, t_\nu}^{\delta^{18}\text{O}} \\ y_{i_3, t_\nu}^{\delta^{18}\text{O}} \\ y_{i_4, t_\nu}^{\delta^{18}\text{O}} \\ y_{i_1, t_\nu}^{\delta^{13}\text{C}} \\ y_{i_2, t_\nu}^{\delta^{13}\text{C}} \\ y_{i_3, t_\nu}^{\delta^{13}\text{C}} \\ y_{i_4, t_\nu}^{\delta^{13}\text{C}} \end{bmatrix}}_{y_{t_\nu} \in \mathbb{R}^{8 \times 1}} = \underbrace{\begin{bmatrix} 1 & 0 \\ 1 & 0 \\ 1 & 0 \\ 1 & 0 \\ 0 & 1 \\ 0 & 1 \\ 0 & 1 \\ 0 & 1 \end{bmatrix}}_{Z \in \mathbb{R}^{8 \times 2}} \underbrace{\begin{bmatrix} \mu_{t_\nu}^{\delta^{18}\text{O}} \\ \mu_{t_\nu}^{\delta^{13}\text{C}} \end{bmatrix}}_{\mu_{t_\nu} \in \mathbb{R}^{2 \times 1}} + \underbrace{\begin{bmatrix} \varepsilon_{i_1, t_\nu}^{\delta^{18}\text{O}} \\ \varepsilon_{i_2, t_\nu}^{\delta^{18}\text{O}} \\ \varepsilon_{i_3, t_\nu}^{\delta^{18}\text{O}} \\ \varepsilon_{i_4, t_\nu}^{\delta^{18}\text{O}} \\ \varepsilon_{i_1, t_\nu}^{\delta^{13}\text{C}} \\ \varepsilon_{i_2, t_\nu}^{\delta^{13}\text{C}} \\ \varepsilon_{i_3, t_\nu}^{\delta^{13}\text{C}} \\ \varepsilon_{i_4, t_\nu}^{\delta^{13}\text{C}} \end{bmatrix}}_{\varepsilon_{t_\nu} \in \mathbb{R}^{8 \times 1}}.$$

The distribution assumption is as above for the univariate model, simply extended to the longer error vector:

$$H_{t_\nu} = \text{diag} \left( \sigma_{\varepsilon, i_1, \delta^{18}O}^2, \sigma_{\varepsilon, i_2, \delta^{18}O}^2, \sigma_{\varepsilon, i_3, \delta^{18}O}^2, \sigma_{\varepsilon, i_4, \delta^{18}O}^2, \sigma_{\varepsilon, i_1, \delta^{13}C}^2, \sigma_{\varepsilon, i_2, \delta^{13}C}^2, \sigma_{\varepsilon, i_3, \delta^{13}C}^2, \sigma_{\varepsilon, i_4, \delta^{13}C}^2 \right),$$

and the relation between  $t_\nu$  and  $i_{(\cdot)}$  is as before the mapping “study  $i_{(\cdot)}$  provided the data point  $y_{i_{\cdot}, t_\nu}$  for time stamp  $t_\nu$ .”

The transition equation for the unobserved component  $\mu$  is given as follows.

$$\underbrace{\begin{bmatrix} \mu_{t_\nu + \Delta t_\nu}^{\delta^{18}O} \\ \mu_{t_\nu + \Delta t_\nu}^{\delta^{13}C} \end{bmatrix}}_{\mu_{t_\nu + \Delta t_\nu} \in \mathbb{R}^{2 \times 1}} = \underbrace{\begin{bmatrix} 1 & 0 \\ 0 & 1 \end{bmatrix}}_{T \in \mathbb{R}^{2 \times 2}} \underbrace{\begin{bmatrix} \mu_{t_\nu}^{\delta^{18}O} \\ \mu_{t_\nu}^{\delta^{13}C} \end{bmatrix}}_{\mu_{t_\nu} \in \mathbb{R}^{2 \times 1}} + \underbrace{\begin{bmatrix} \eta_{j, t_\nu}^{\delta^{18}O} \\ \eta_{j, t_\nu}^{\delta^{13}C} \end{bmatrix}}_{\eta_{t_\nu} \in \mathbb{R}^{2 \times 1}}.$$

In the transition equation, we allow for correlation of the transition error from the unobserved component in  $\delta^{18}O$  with the one in  $\delta^{13}C$ :  $\eta_{t_\nu} \stackrel{i.i.d.}{\sim} \mathbf{N}(0, Q_{t_\nu})$ ,

$$Q_{t_\nu} = \begin{bmatrix} \sigma_{\eta, \delta^{18}O, j}^2 \Delta t_\nu^{\delta^{18}O} & \rho_j \sigma_{\eta, \delta^{18}O, j} \sigma_{\eta, \delta^{13}C, j} \min\{\Delta t_\nu^{\delta^{18}O}, \Delta t_\nu^{\delta^{13}C}\} \\ \rho_j \sigma_{\eta, \delta^{18}O, j} \sigma_{\eta, \delta^{13}C, j} \min\{\Delta t_\nu^{\delta^{18}O}, \Delta t_\nu^{\delta^{13}C}\} & \sigma_{\eta, \delta^{13}C, j}^2 \Delta t_\nu^{\delta^{13}C} \end{bmatrix},$$

where the  $j$  indicate the climate state according to Table 4, and

$$\Delta t_\nu^{(\delta^{18}O, \delta^{13}C)} = \begin{cases} \Delta t_\nu, & \text{if preceding obs at } t_{\nu-1} \text{ is not NA,} \\ \Delta t_\nu + \Delta t_{\nu-1}^{(\delta^{18}O, \delta^{13}C)}, & \text{if preceding obs at } t_{\nu-1} \text{ is NA.} \end{cases}$$

## B Measurement equation variances by benthic foraminifera species

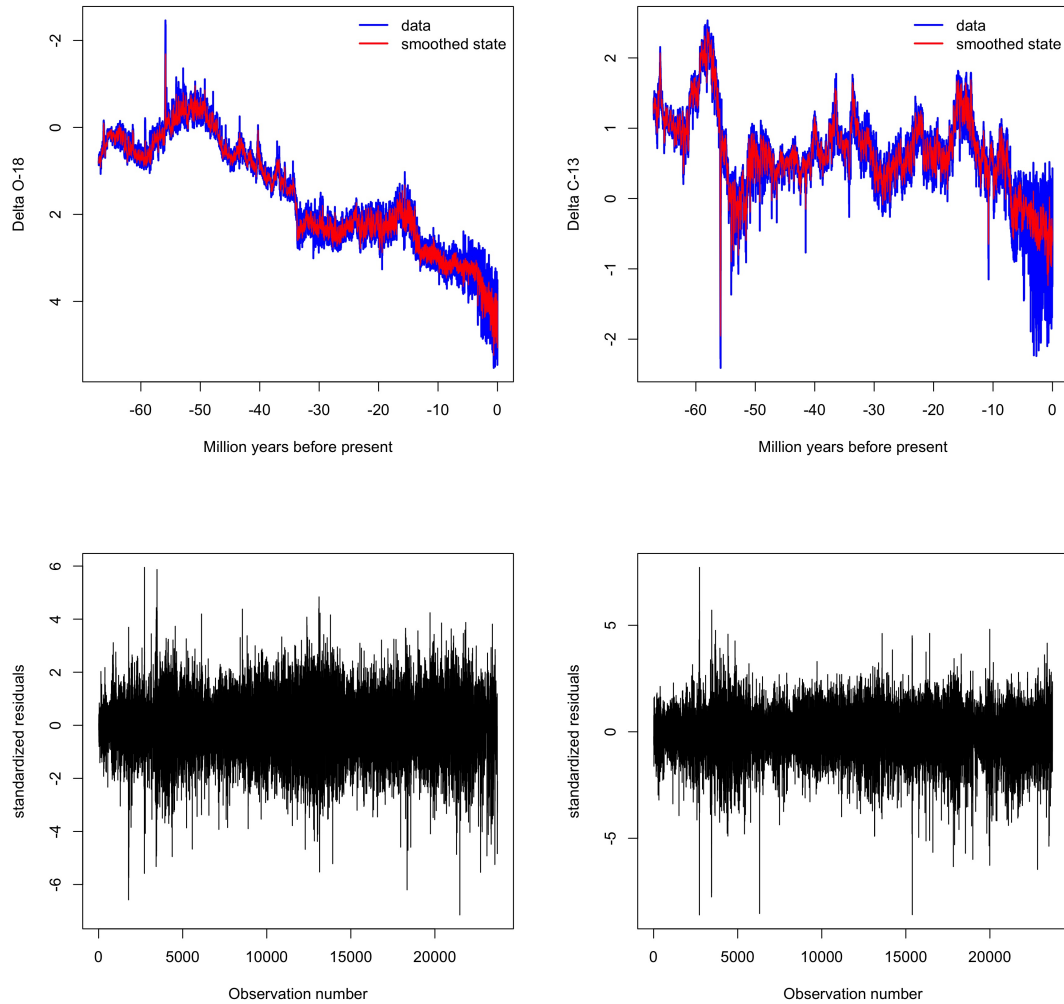


Figure 8: Top left panel:  $\delta^{18}\text{O}$  data (blue) and smoothed state  $\mathbb{E}[\mu_{t+\Delta t}|\{y_s, s \leq \sum \Delta t\}]$  (red) according to model (4) from Kalman smoothing recursions. Top right panel: same for  $\delta^{13}\text{C}$ . Note that the  $y$ -axis for  $\delta^{18}\text{O}$  is reversed, following common practice. Bottom left panel: standardized residuals for  $\delta^{18}\text{O}$ , bottom right panel: standardized residuals for  $\delta^{13}\text{C}$ .

Table 12: Maximum likelihood estimates of model (4). Standard errors in parentheses. “Species” refers to the entry in column “benthic Species” in tab “Table S33” of the data file `aba6853_tables_s8_s34.xlsx` of Westerhold et al. (2020). BIC: Bayes information criterion.

Variance	Species	No. obs.	$\delta^{18}\text{O}$	No. obs.	$\delta^{13}\text{C}$
$\sigma_{\varepsilon,1}^2$	“NTRUE”	6949	0.0120 (0.0003)	6949	0.0093 (0.0002)
$\sigma_{\varepsilon,2}^2$	“OUMB”	240	0.0510 (0.0052)	56	0.0524 (0.0113)
$\sigma_{\varepsilon,3}^2$	“CSUBS or CEOCEA, not specified in publication”	301	0.0125 (0.0016)	301	0.0162 (0.0019)
$\sigma_{\varepsilon,4}^2$	“CPRAE”	136	0.0165 (0.0030)	136	0.0203 (0.0034)
$\sigma_{\varepsilon,5}^2$	“CSPP”	2310	0.0188 (0.0007)	2310	0.0332 (0.0011)
$\sigma_{\varepsilon,6}^2$	CSPP >250		0.0177 (0.0017)		0.0073 (0.0008)
	“CSPP, >250”	353		353	
	“CSPP, specimen >250 $\mu\text{m}$ ”	10		10	
$\sigma_{\varepsilon,7}^2$	CSPP other		0.0209 (0.0042)		0.0231 (0.0045)
	“CSPP, whole specimen”	25		25	
	“CSPP, 150-250”	2		2	
	“CSPP, >250, Reruns”	58		58	
$\sigma_{\varepsilon,8}^2$	“CGRIM”	318	0.0294 (0.0028)	318	0.0203 (0.0019)
$\sigma_{\varepsilon,9}^2$	“CHAVA”	92	0.0246 (0.0046)	92	0.0111 (0.0024)
$\sigma_{\varepsilon,10}^2$	“CMUND”	4380	0.0105 (0.0003)	4380	0.0126 (0.0003)
$\sigma_{\varepsilon,11}^2$	“PWUEL; CMUND”	4249	0.0114 (0.0004)	4249	0.0084 (0.0003)
$\sigma_{\varepsilon,12}^2$	“PWUEL (eitherCKULL or PWUEL)”	807	0.0125 (0.0007)	807	0.0129 (0.0007)
$\sigma_{\varepsilon,13}^2$	“PWUEL”	3405	0.0592 (0.0017)	3407	0.1458 (0.0039)
$\sigma_{\varepsilon,14}^2$	“CKULL”	255	0.0551 (0.0054)	254	0.0678 (0.0074)
$\sigma_{\varepsilon,15}^2$	“UVIG”	149	0.0498 (0.0064)	133	0.0591 (0.0010)
$\sigma_{\varepsilon,16}^2$	“GORB”	30	0.0604 (0.0167)	0	—
$\sigma_{\varepsilon,17}^2$	“PMURR”	91	0.0719 (0.0115)	0	—
$\sigma_{\varepsilon,18}^2$	“NUMB”	65	0.0741 (0.0139)	65	0.4352 (0.0789)
$\sigma_{\varepsilon,19}^2$	“CBRA”	22	0.0408 (0.0139)	22	0.0733 (0.0242)
$\sigma_{\varepsilon,20}^2$	“CCIC”	12	0.0657 (0.0284)	12	0.1171 (0.0499)
$\sigma_{\eta}^2$			1.6051 (0.0485)		1.1171 (0.0499)
log-likelihood		24259	9169.53	23939	8855.73
BIC			-18127.50		-17520.06

## C Unobserved components and residuals plots for model (5)

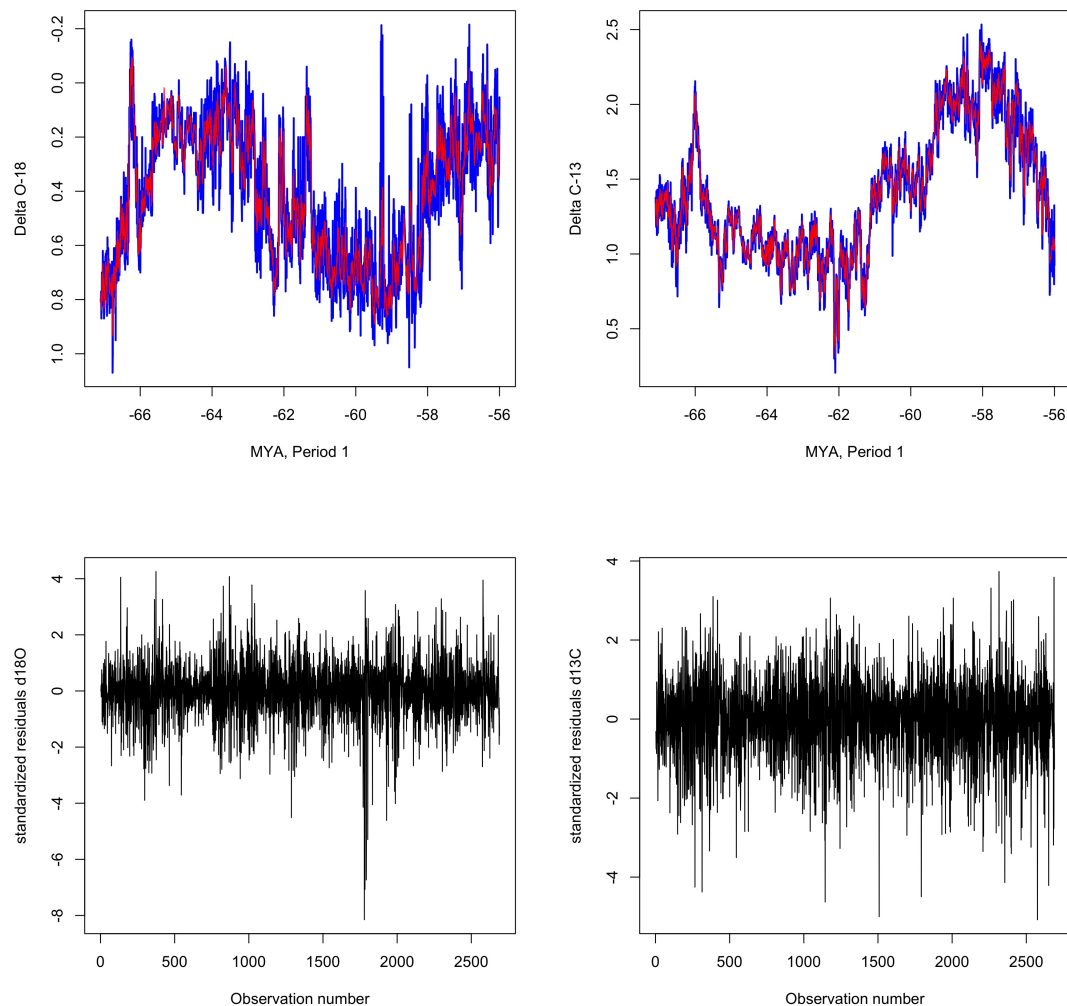


Figure 9: Top left panel:  $\delta^{18}\text{O}$  data (blue) and smoothed state  $\mathbb{E}[\mu_{t+\Delta t}|\{y_s, s \leq \sum \Delta t\}]$  (red) according to model (5) for the first climate state from Kalman smoothing recursions. Top right panel: same for  $\delta^{13}\text{C}$ . Note that the  $y$ -axis for  $\delta^{18}\text{O}$  is reversed, following common practice. Bottom left panel: standardized residuals for  $\delta^{18}\text{O}$ , bottom right panel: standardized residuals for  $\delta^{13}\text{C}$ .

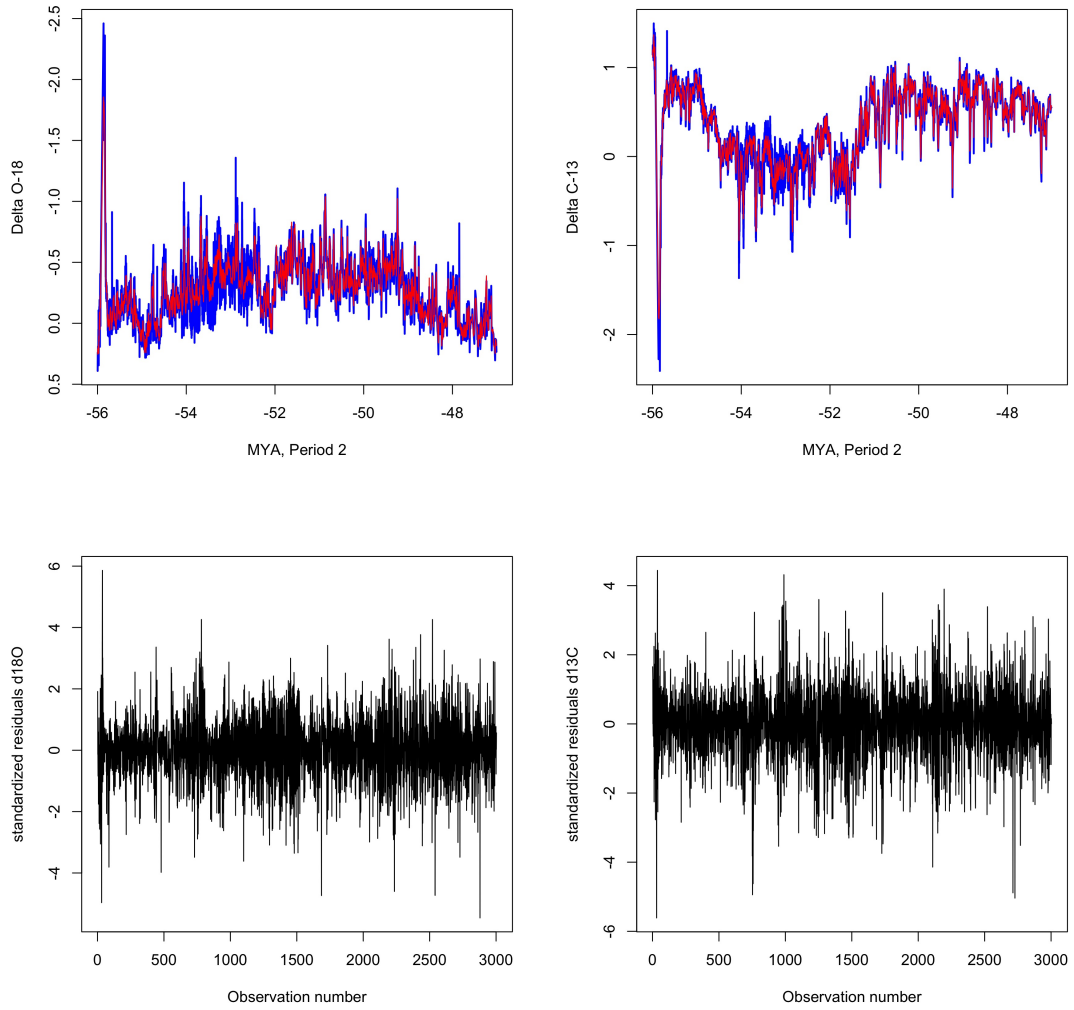


Figure 10: Top left panel:  $\delta^{18}\text{O}$  data (blue) and smoothed state  $\mathbb{E}[\mu_{t+\Delta t} | \{y_s, s \leq \sum \Delta t\}]$  (red) according to model (5) for the second climate state from Kalman smoothing recursions. Top right panel: same for  $\delta^{13}\text{C}$ . Note that the  $y$ -axis for  $\delta^{18}\text{O}$  is reversed, following common practice. Bottom left panel: standardized residuals for  $\delta^{18}\text{O}$ , bottom right panel: standardized residuals for  $\delta^{13}\text{C}$ .

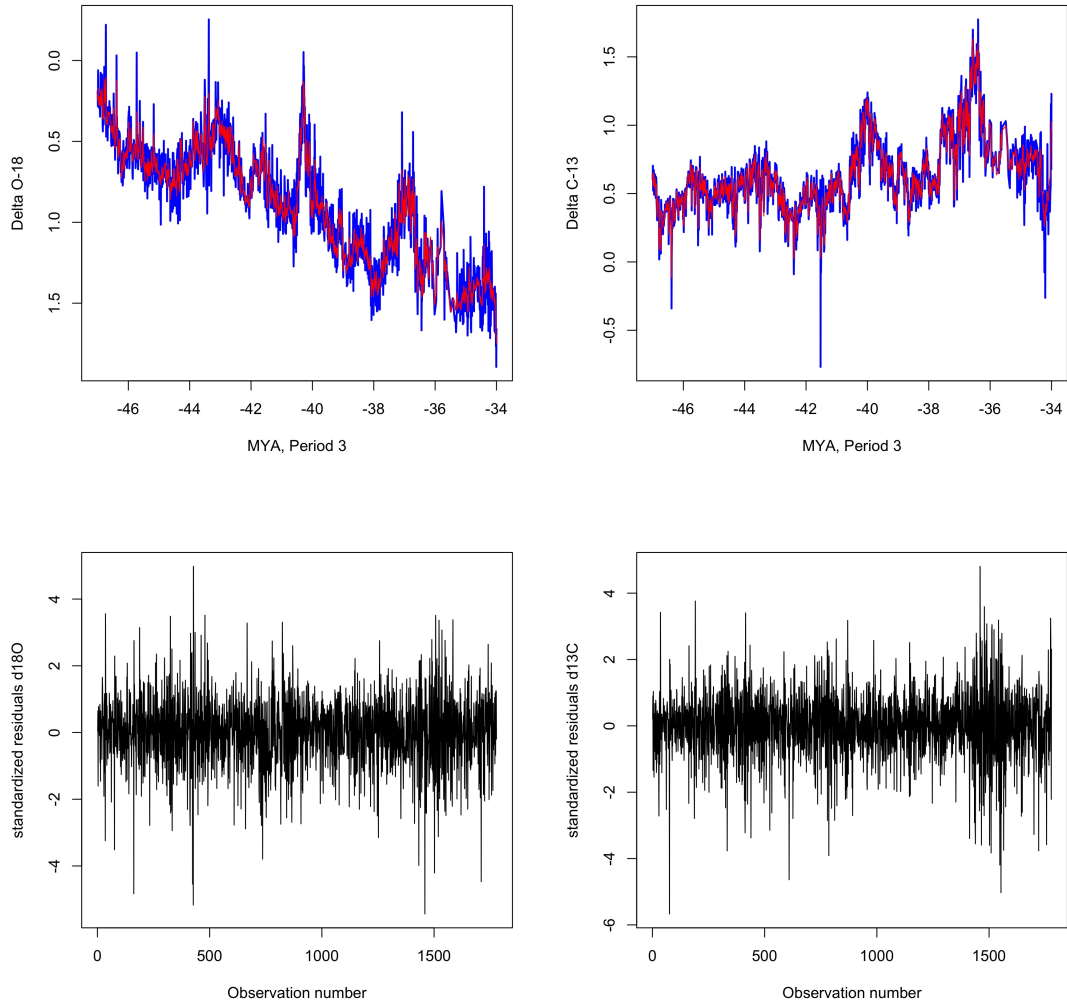


Figure 11: Top left panel:  $\delta^{18}\text{O}$  data (blue) and smoothed state  $\mathbb{E}[\mu_{t+\Delta t}|\{y_s, s \leq \sum \Delta t\}]$  (red) according to model (5) for the third climate state from Kalman smoothing recursions. Top right panel: same for  $\delta^{13}\text{C}$ . Note that the  $y$ -axis for  $\delta^{18}\text{O}$  is reversed, following common practice. Bottom left panel: standardized residuals for  $\delta^{18}\text{O}$ , bottom right panel: standardized residuals for  $\delta^{13}\text{C}$ .

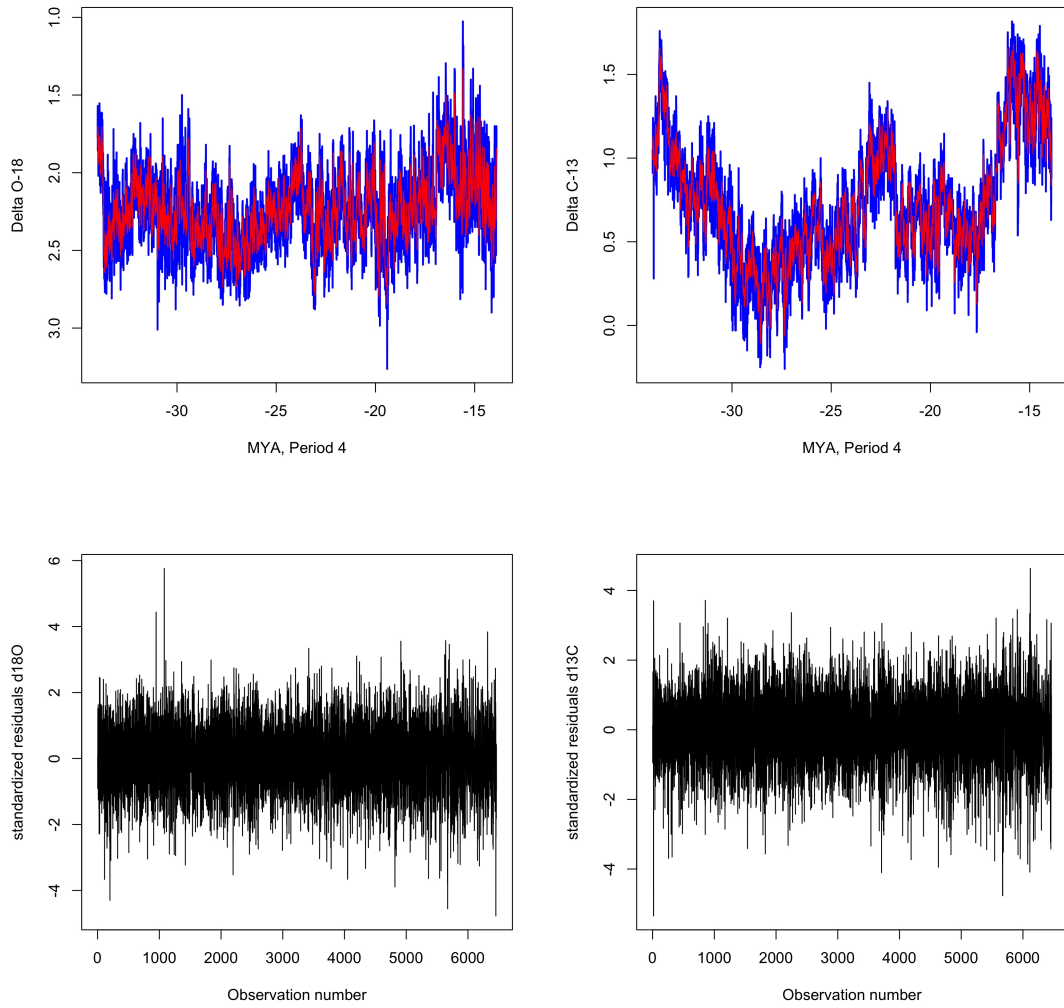


Figure 12: Top left panel:  $\delta^{18}\text{O}$  data (blue) and smoothed state  $\mathbb{E}[\mu_{t+\Delta t}|\{y_s, s \leq \sum \Delta t\}]$  (red) according to model (5) for the fourth climate state from Kalman smoothing recursions. Top right panel: same for  $\delta^{13}\text{C}$ . Note that the  $y$ -axis for  $\delta^{18}\text{O}$  is reversed, following common practice. Bottom left panel: standardized residuals for  $\delta^{18}\text{O}$ , bottom right panel: standardized residuals for  $\delta^{13}\text{C}$ .



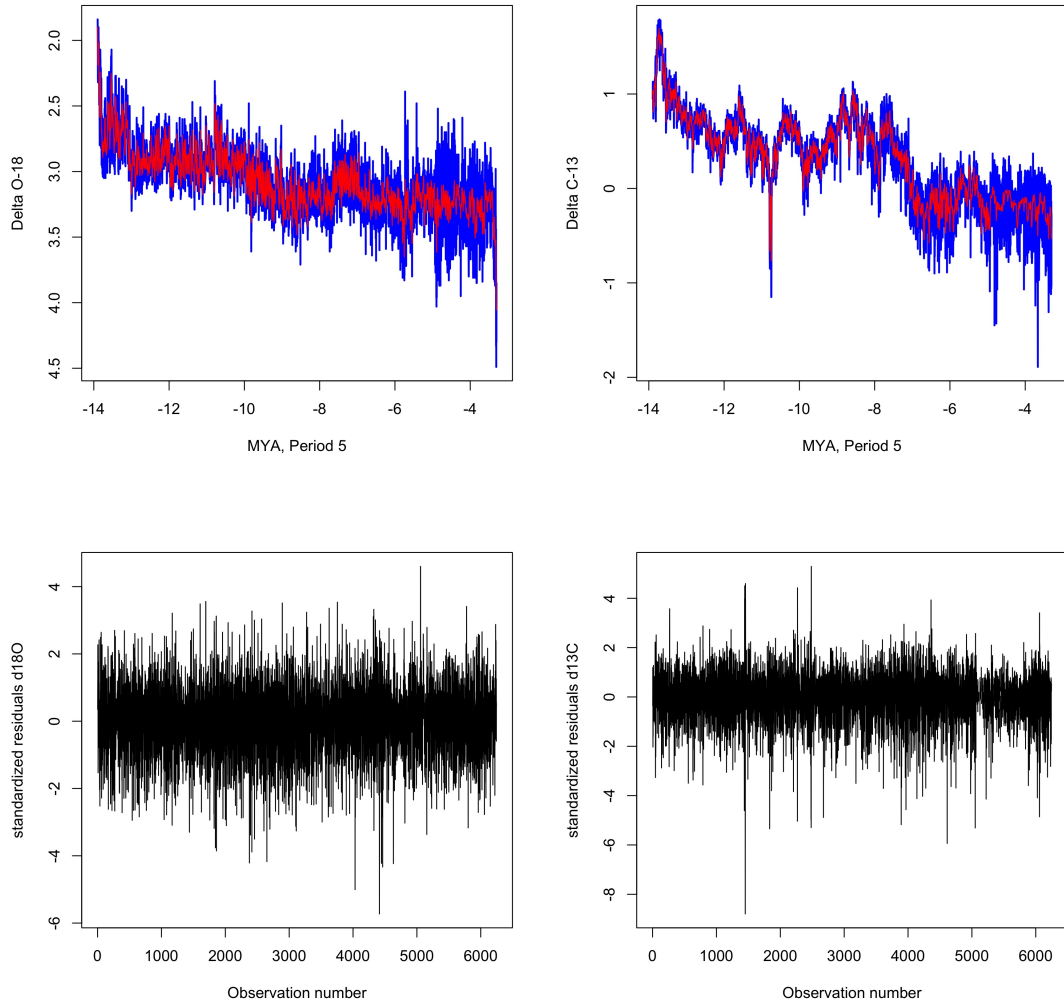


Figure 13: Top left panel:  $\delta^{18}\text{O}$  data (blue) and smoothed state  $\mathbb{E}[\mu_{t+\Delta t} | \{y_s, s \leq \sum \Delta t\}]$  (red) according to model (5) for the fifth climate state from Kalman smoothing recursions. Top right panel: same for  $\delta^{13}\text{C}$ . Note that the  $y$ -axis for  $\delta^{18}\text{O}$  is reversed, following common practice. Bottom left panel: standardized residuals for  $\delta^{18}\text{O}$ , bottom right panel: standardized residuals for  $\delta^{13}\text{C}$ .

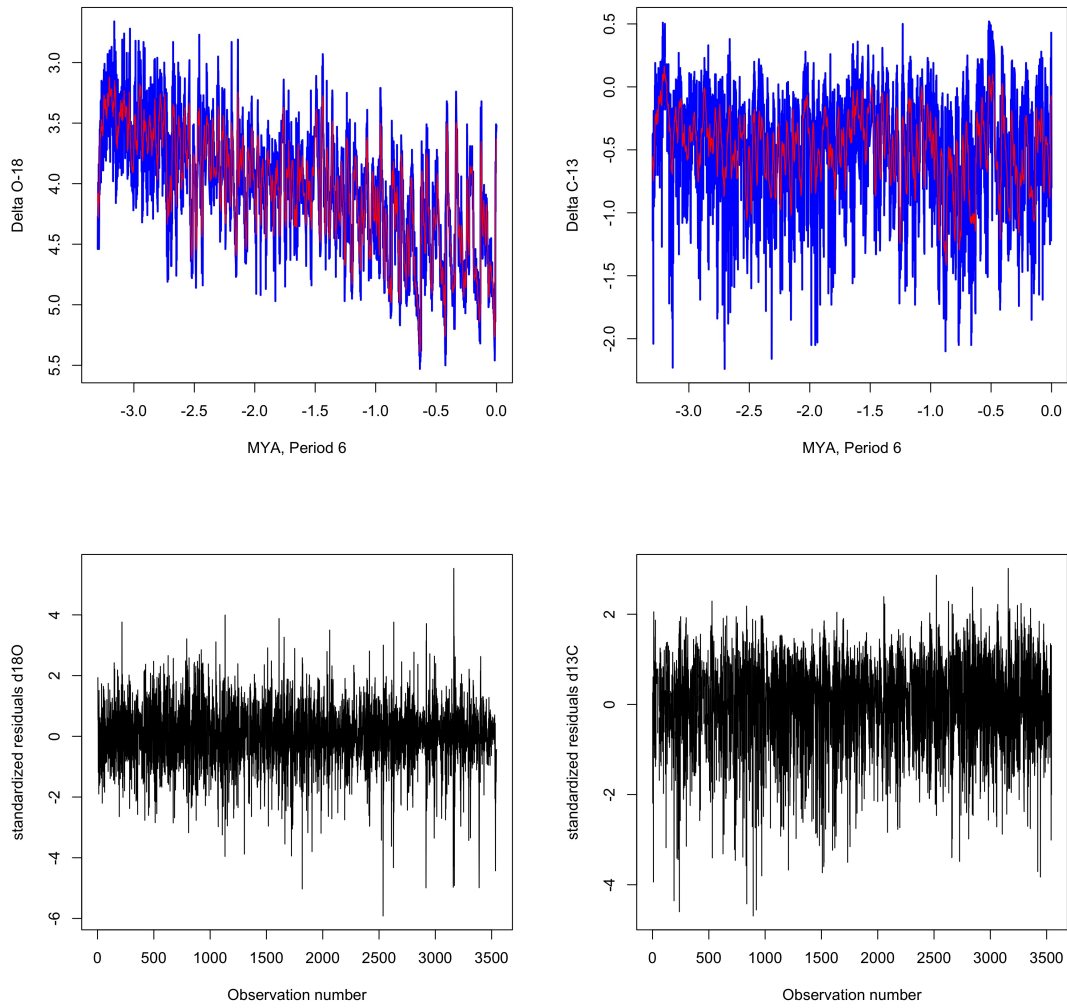


Figure 14: Top left panel:  $\delta^{18}\text{O}$  data (blue) and smoothed state  $\mathbb{E}[\mu_{t+\Delta t}|\{y_s, s \leq \sum \Delta t\}]$  (red) according to model (5) for the sixth climate state from Kalman smoothing recursions. Top right panel: same for  $\delta^{13}\text{C}$ . Note that the  $y$ -axis for  $\delta^{18}\text{O}$  is reversed, following common practice. Bottom left panel: standardized residuals for  $\delta^{18}\text{O}$ , bottom right panel: standardized residuals for  $\delta^{13}\text{C}$ .

## References

- Bagchi, S. and S. K. Mitra (1996). The nonuniform discrete Fourier transform and its applications in filter design. I. 1-D. *IEEE Transactions on Circuits and Systems II: Analog and Digital Signal Processing* 43(6), 422–433.
- Bell, W. (1984). Signal extraction for nonstationary time series. *The Annals of Statistics* 12(2), 646–664.
- Doornik, J. (2021). *An Introduction to OxMetrics 9*. Timberlake Consultants.
- Durbin, J. and S. J. Koopman (2012). *Time Series Analysis by State Space Methods* (2 ed.). Oxford University Press.
- Gómez, V. (1999). Three equivalent methods for filtering finite nonstationary time series. *Journal of Business & Economic Statistics* 17(1), 109–116.
- Gómez, V. (2001). The use of butterworth filters for trend and cycle estimation in economic time series. *Journal of Business & Economic Statistics* 19(3), 365–373.
- Harvey, A. and S. J. Koopman (2000). Signal extraction and the formulation of unobserved components models. *The Econometrics Journal* 3(1), 84–107.
- Harvey, A. and S. J. Koopman (2009). Unobserved components models in economics and finance. *IEEE Control Systems Magazine* 29(6), 71–81.
- Harvey, A. C. (1989). *Forecasting, Structural Time Series Models and the Kalman Filter*. Cambridge: Cambridge University Press.
- Harvey, A. C. and T. M. Trimbur (2003). General model-based filters for extracting cycles and trends in economic time series. *Review of Economics and Statistics* 85(2), 244–255.
- Helske, J. (2017). KFAS: Exponential family state space models in R. *Journal of Statistical Software* 78, 1–38.
- Helske, J. (2019). Package “KFAS”: Kalman filter and smoother for exponential family state-space models. Technical report, CRAN repository, version 1.3.4.
- Karatzas, I. and S. E. Shreve (1991). *Brownian Motion and Stochastic Calculus* (second ed.). Springer.
- Turner, S. K. (2014). Pliocene switch in orbital-scale carbon cycle/climate dynamics. *Paleoceanography* 29(12), 1256–1266.
- Westerhold, T., N. Marwan, A. J. Drury, D. Liebrand, C. Agnini, E. Anagnostou, J. S. Barnet, S. M. Bohaty, D. De Vleeschouwer, F. Florindo, et al. (2020). An astronomically dated record of earth’s climate and its predictability over the last 66 million years. *Science* 369(6509), 1383–1387.
- Whittle, P. (1983). *Prediction and Regulation by Linear Least-Square Methods* (second ed.). University of Minnesota Press.
- Zachos, J., M. Pagani, L. Sloan, E. Thomas, and K. Billups (2001). Trends, rhythms, and aberrations in global climate 65 ma to present. *Science* 292(5517), 686–693.